



*Citation for published version:*

Zeidler, A, Salmon, P, Whittaker, D, Pizzey, K & Hannon, AC 2017, 'Topological Ordering and Viscosity in the Glass-Forming Ge-Se System: The Search for a Structural or Dynamical Signature of the Intermediate Phase', *Frontiers in Materials*, vol. 4, no. 32, 32. <https://doi.org/10.3389/fmats.2017.00032>

*DOI:*

[10.3389/fmats.2017.00032](https://doi.org/10.3389/fmats.2017.00032)

*Publication date:*

2017

*Document Version*

Peer reviewed version

[Link to publication](#)

*Publisher Rights*

CC BY

## University of Bath

**General rights**

Copyright and moral rights for the publications made accessible in the public portal are retained by the authors and/or other copyright owners and it is a condition of accessing publications that users recognise and abide by the legal requirements associated with these rights.

**Take down policy**

If you believe that this document breaches copyright please contact us providing details, and we will remove access to the work immediately and investigate your claim.

# Topological Ordering and Viscosity in the Glass-Forming Ge-Se System: The Search for a Structural or Dynamical Signature of the Intermediate Phase

Anita Zeidler<sup>1</sup>, Philip S. Salmon<sup>1</sup>, Dean A. J. Whittaker<sup>1</sup>,  
Keiron J. Pizzey<sup>1</sup>, Alex C. Hannon<sup>2</sup>

<sup>1</sup> Department of Physics, University of Bath, Bath BA2 7AY, UK

<sup>2</sup> ISIS Facility, Rutherford Appleton Laboratory, Chilton, Didcot, Oxon OX11 0QX, UK

**Abstract.** The topological ordering of the network structure in vitreous  $\text{Ge}_x\text{Se}_{1-x}$  was investigated across most of the glass-forming region ( $0 \leq x \leq 0.4$ ) by using high-resolution neutron diffraction to measure the Bhatia-Thornton number-number partial structure factor. This approach gives access to the composition dependence of the mean coordination number  $\bar{n}$  and correlation lengths associated with the network ordering. The thermal properties of the samples were also measured by using temperature-modulated differential scanning calorimetry. The results do not point to a structural origin of the so-called intermediate phase, which in our work is indicated for the composition range  $0.175(8) \leq x \leq 0.235(8)$  by a vanishingly-small non-reversing enthalpy near the glass transition. The midpoint of this range coincides with the mean-field expectation of a floppy-to-rigid transition at  $x = 0.20$ . The composition dependence of the liquid viscosity, as taken from the literature, was also investigated to look for a dynamical origin of the intermediate phase, using the Mauro-Yue-Ellison-Gupta-Allan (MYEGA) model to estimate the viscosity at the liquidus temperature. The evidence points to a maximum in the viscosity at the liquidus temperature, and a minimum in the fragility index, for the range  $0.20 \leq x \leq 0.22$ . The utility of the intermediate phase as a predictor of the material properties in network glass-forming systems is discussed.

**Keywords:** Chalcogenide glass, neutron diffraction, viscosity, fragility index, intermediate phase, material properties

PACS numbers: 61.43.Fs, 61.05.fm, 66.20.Ej, 64.70.dj

Submitted to: *Frontiers in Materials: Glass Science*

## 1. INTRODUCTION

The structural disorder associated with covalently-bonded network-forming glassy materials gives rise to a diversity of material properties, which leads to the importance of glass in multiple technologies (Cusack 1987; Elliott 1990; Feltz 1993). It is possible to predict many of the structure-related properties of these materials by using constraint-counting theory, where the constraints originate from the bond-stretching and bond-bending interatomic forces associated with the covalent bonds of network-forming motifs (Phillips 1979; Thorpe 1983). As the type and proportion of network-forming motifs is altered, the network topology will respond accordingly. Hence, the connectivity and properties of covalently-bonded network-forming glasses can be manipulated systematically by altering their composition.

On the basis of mean-field constraint-counting theory, a network is predicted to undergo the transition from an elastically floppy to a stressed-rigid state when the mean number of Lagrangian bonding constraints per atom  $N_c$  is equal to three, i.e., the number of degrees of freedom per atom in three dimensions. Floppy phases are under-constrained ( $N_c < 3$ ), and stressed-rigid phases are over-constrained ( $N_c > 3$ ). For a system in which all of the bond-stretching and bond-bending constraints are intact and there are no dangling bonds, the transition at  $N_c = 3$  corresponds to a mean coordination number  $\bar{n} = 2.40$  where the network is isostatically rigid and stress free (Phillips 1979; Thorpe 1983). If the network can self-organise and thereby lower the free energy at the temperature of its formation by the incorporation of structural configurations that minimise the occurrence of over-constrained regions, then it is postulated that two transitions can appear (Thorpe et al., 2000). In this case, the floppy and stressed-rigid phases are separated by a composition range known as the intermediate phase where the network is isostatically rigid and stress free. The compositional width of this phase is thought to be related to structural variability, i.e., the ability of a network to incorporate a range of structural motifs (Massobrio et al., 2009; Sartbaeva et al., 2007). In temperature-modulated differential scanning calorimetry (TMDSC) experiments, the existence of a stress-free intermediate-phase is inferred from the non-reversing part of the measured enthalpy  $\Delta H_{nr}$ , which takes a value close to zero near the glass transition temperature  $T_g$  (Boolchand et al., 2001b; Wang et al., 2000). The structural motifs of the intermediate phase are expected to yield  $N_c = 3$  such that the network is optimally constrained to avoid stress.  $\text{Ge}_x\text{Se}_{1-x}$  ( $0 \leq x \leq 1$ ) is a prototypical covalently-bonded network-forming system for which the intermediate phase spans a wide composition window, usually reported as  $0.20 \lesssim x \lesssim 0.26$  (Bhosle et al., 2012b, Boolchand et al., 2001a; Boolchand et al., 2007).

The first objective of this paper is to search for a structural origin of the intermediate phase by performing a set of neutron diffraction experiments on vitreous  $\text{Ge}_x\text{Se}_{1-x}$  across the glass-forming region  $0 \leq x \leq 0.43$  (Azoulay et al., 1975). The experiments used samples containing Ge and Se of natural isotopic abundance, for which the coherent neutron scattering lengths take similar values, i.e.,  $b_{\text{Ge}} = 8.185(20)$  fm

73 and  $b_{\text{Se}} = 7.970(9)$  fm (Sears 1992). In consequence, the Bhatia-Thornton (1970)  
 74 number-number partial structure factor  $S_{\text{NN}}(q)$  is measured to an excellent level of  
 75 approximation, where  $q$  denotes the magnitude of the scattering vector (Salmon 2007a).  
 76 This function and its Fourier transform, the number-number partial pair-distribution  
 77 function  $g_{\text{NN}}(r)$ , do not distinguish between the chemical species that occupy the atomic  
 78 sites in a glass-forming network structure, and therefore yield important information on  
 79 the topological ordering (Petri et al., 1999; Salmon 1992; Salmon and Liu 1994). For  
 80 example, the mean coordination number  $\bar{n}$  is obtained directly from  $g_{\text{NN}}(r)$ . In addition,  
 81 the peak positions and widths in  $S_{\text{NN}}(q)$  describe the atomic ordering in a glass network  
 82 on different length scales (Salmon 1994; Salmon et al., 2005; Zeidler and Salmon 2016).  
 83 One of these length scales is associated with an intermediate range, and manifests itself  
 84 by the appearance of a first sharp diffraction peak (FSDP) in  $S_{\text{NN}}(q)$  at  $q_{\text{FSDP}}$ , where  
 85  $q_{\text{FSDP}}r_{\text{nn}} \simeq 2.2 - 2.8$  for glassy  $\text{Ge}_x\text{Se}_{1-x}$  and  $r_{\text{nn}}$  is the nearest-neighbour bond distance.  
 86 Another length scale is associated with ordering on an extended range, and manifests  
 87 itself by the appearance of a principal peak in  $S_{\text{NN}}(q)$  at  $q_{\text{PP}}$ , where  $q_{\text{PP}}r_{\text{nn}} \simeq 4.5 - 4.8$   
 88 for glassy  $\text{Ge}_x\text{Se}_{1-x}$ . A competition between the ordering on these two length scales for  
 89 different classes of binary glass-forming melts influences their relative fragility (Salmon  
 90 et al., 2006; Salmon 2007b; Salmon and Zeidler 2013). The present neutron diffraction  
 91 work complements previous investigations on the structure of intermediate phase glasses  
 92 using neutron diffraction (Ramesh Rao et al., 1998), x-ray diffraction (Sharma et al.,  
 93 2005; Wang et al., 2004), anomalous x-ray diffraction (Hosokawa et al., 2003, 2011);  
 94 or a combination of high-energy x-ray diffraction and extended x-ray absorption fine  
 95 structure (EXAFS) spectroscopy (Shatnawi et al., 2008).

96 The second objective of this paper is to investigate the viscosity at the liquidus  
 97 temperature in the  $\text{Ge}_x\text{Se}_{1-x}$  system by using the Mauro-Yue-Ellison-Gupta-Allan  
 98 (MYEGA) model (Mauro et al., 2009) to search for a dynamical signature of the  
 99 intermediate phase. For a given composition, the equilibrium liquid will have more  
 100 thermal energy than the supercooled liquid, which should give a greater opportunity for  
 101 reorganization of the network structure. The self-organization that occurs on quenching  
 102 to form a stress-free intermediate-phase glass should therefore manifest itself in the  
 103 dynamics of the liquid state at the liquidus temperature  $T_L$ , and the temperature-  
 104 dependent viscosity  $\eta(T)$  is an important measure of the dynamics for a glass-forming  
 105 material.

106 The paper is organised as follows. The essential neutron diffraction theory is  
 107 outlined in Section 2. The experimental method is described in Section 3 and the neutron  
 108 diffraction results are given in Section 4. The composition dependence of the viscosity  
 109 and fragility index is described in Section 5. The results are discussed in Section 6,  
 110 where the composition dependence of the glass structure is considered, along with the  
 111 utility of the intermediate phase as a predictor of material properties. Conclusions are  
 112 drawn in Section 7.

## 113 2. THEORY

114 The total structure factor measured in a neutron diffraction experiment on glassy  
115  $\text{Ge}_x\text{Se}_{1-x}$  is given by (Fischer et al., 2006)

$$116 \quad S(q) = \frac{1}{\langle b \rangle^2} \left[ x^2 b_{\text{Ge}}^2 S_{\text{GeGe}}(q) + 2x(1-x)b_{\text{Ge}}b_{\text{Se}}S_{\text{GeSe}}(q) + (1-x)^2 b_{\text{Se}}^2 S_{\text{SeSe}}(q) \right] \quad (1)$$

117 where  $S_{\alpha\beta}(q)$  is the partial structure factor for chemical species  $\alpha$  and  $\beta$ , and  $\langle b \rangle =$   
118  $xb_{\text{Ge}} + (1-x)b_{\text{Se}}$  is the mean coherent neutron scattering length. The close similarity  
119 between the  $b_{\text{Ge}}$  and  $b_{\text{Se}}$  values for Ge and Se of natural isotopic abundance means that  
120  $S(q) \simeq S_{\text{NN}}(q)$  to an excellent level of approximation (Salmon 2007a), where  $S_{\text{NN}}(q)$  is  
121 given by Eq. (1) if  $b_{\text{Ge}} = b_{\text{Se}}$ . The total pair-distribution function  $g(r)$  follows from the  
122 Fourier transform relation

$$123 \quad g(r) - 1 = \frac{1}{2\pi^2 \rho r} \int_0^\infty dq q [S(q) - 1] M(q) \sin(qr) \quad (2)$$

124 where  $\rho$  is the atomic number density. The measurement window of a diffractometer  
125 is limited to a maximum scattering vector  $q_{\text{max}}$  such that  $M(q \leq q_{\text{max}}) = 1$ ,  $M(q >$   
126  $q_{\text{max}}) = 0$ .

127 If  $q_{\text{max}}$  is sufficiently large that the effect of  $M(q)$  can be neglected, the overall mean  
128 coordination number for the spatial range  $r_1 \leq r \leq r_2$  follows from the expression

$$\begin{aligned} \bar{n} &= 4\pi\rho \int_{r_1}^{r_2} dr r^2 g(r) \\ &= \frac{1}{\langle b \rangle^2} \left[ xb_{\text{Ge}} (b_{\text{Ge}}\bar{n}_{\text{Ge}}^{\text{Ge}} + b_{\text{Se}}\bar{n}_{\text{Ge}}^{\text{Se}}) + (1-x)b_{\text{Se}} (b_{\text{Se}}\bar{n}_{\text{Se}}^{\text{Se}} + b_{\text{Ge}}\bar{n}_{\text{Se}}^{\text{Ge}}) \right], \end{aligned} \quad (3)$$

129 where  $\bar{n}_\alpha^\beta$  is the mean coordination number of chemical species  $\beta$  about chemical species  
130  $\alpha$  for the range  $r_1 \leq r \leq r_2$ . In the case when  $b_{\text{Ge}} = b_{\text{Se}}$ , Eq. (3) reduces to the expression

$$131 \quad \bar{n} = 4\pi\rho \int_{r_1}^{r_2} dr r^2 g_{\text{NN}}(r) = x (\bar{n}_{\text{Ge}}^{\text{Ge}} + \bar{n}_{\text{Ge}}^{\text{Se}}) + (1-x) (\bar{n}_{\text{Se}}^{\text{Se}} + \bar{n}_{\text{Se}}^{\text{Ge}}). \quad (4)$$

132 Then, on the basis of the ‘8-N’ rule in which the Ge and Se atoms are four-fold and  
133 two-fold coordinated, respectively, such that  $\bar{n}_{\text{Ge}} \equiv \bar{n}_{\text{Ge}}^{\text{Ge}} + \bar{n}_{\text{Ge}}^{\text{Se}} = 4$  and  $\bar{n}_{\text{Se}} \equiv \bar{n}_{\text{Se}}^{\text{Se}} + \bar{n}_{\text{Se}}^{\text{Ge}}$   
134  $= 2$ , it follows that

$$135 \quad \bar{n} = 2(1+x). \quad (5)$$

136 The coordination numbers  $\bar{n}_\alpha^\beta$  can be calculated on the basis of a chemically ordered  
137 network (CON) or random covalent network (RCN) model, both of which satisfy the ‘8-  
138 N’ rule (Salmon 2007a). In the CON, Ge-Se bonds are favored such that only Ge-Se and  
139 Se-Se bonds are allowed for  $x < 1/3$  whereas only Ge-Se and Ge-Ge bonds are allowed  
140 for  $x > 1/3$ . The associated coordination numbers are  $\bar{n}_{\text{Ge}}^{\text{Se}} = 4$ ,  $\bar{n}_{\text{Se}}^{\text{Se}} = 2(1-3x)/(1-x)$   
141 and  $\bar{n}_{\text{Ge}}^{\text{Ge}} = 0$  for  $x < 1/3$ ;  $\bar{n}_{\text{Ge}}^{\text{Se}} = 2(1-x)/x$ ,  $\bar{n}_{\text{Se}}^{\text{Se}} = 0$  and  $\bar{n}_{\text{Ge}}^{\text{Ge}} = 2(3x-1)/x$  for  $x > 1/3$ ;  
142 or  $\bar{n}_{\text{Ge}}^{\text{Se}} = 4$  with  $\bar{n}_{\text{Ge}}^{\text{Ge}} = \bar{n}_{\text{Se}}^{\text{Se}} = 0$  at the stoichiometric composition  $x = 1/3$ . In the RCN,  
143 there is a purely statistical distribution of bond types giving  $\bar{n}_{\text{Ge}}^{\text{Se}} = 4(1-x)/(1+x)$ ,  
144  $\bar{n}_{\text{Se}}^{\text{Se}} = 2(1-x)/(1+x)$  and  $\bar{n}_{\text{Ge}}^{\text{Ge}} = 8x/(1+x)$ . Hence, provided the ‘8-N’ rule holds

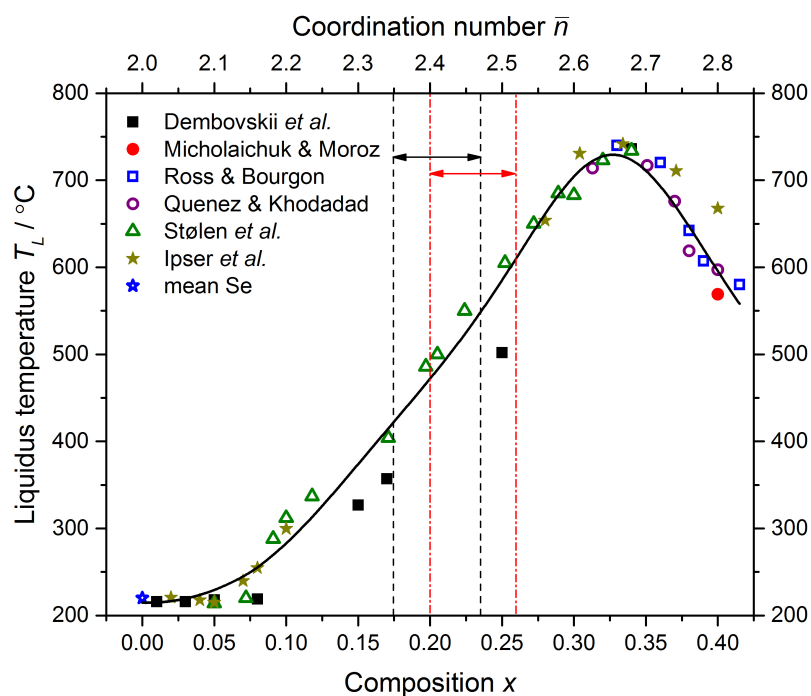


**Figure 1.** The dependence of the liquidus temperature  $T_L$  for the  $\text{Ge}_x\text{Se}_{1-x}$  system on the composition  $x$  and mean coordination number  $\bar{n} = 2(1+x)$ . The data point for Se is a mean of the values reported by Berkes and Myers (1971); Johnson et al. (1986); Morgant and Legendre (1986); Ota and Kunugi (1973); and Stølen et al. (1999). The other data points were taken from Dembovskii et al. (1965); Ipser et al. (1982); Mikolaichuk and Moroz (1986); Quenez and Khodadad (1969); Ross and Bourgon (1969); and Stølen et al. (1999). The solid (black) curve gives a least-squares fit of the measured data sets to an inverse polynomial function. The pairs of vertical dashed (black) or chained (red) lines, and associated horizontal arrows, mark compositions for which  $\Delta H_{nr} \simeq 0$  as found in the present work or in the work of Boolchand et al. (2001a), respectively.

145 for the  $\text{Ge}_x\text{Se}_{1-x}$  system,  $\bar{n}$  will follow from Eq. (5) if an experiment is performed on a  
 146 sample for which  $b_{\text{Ge}} = b_{\text{Se}}$ , or  $\bar{n}$  can be calculated from either the CON or RCN model  
 147 by using Eq. (3) if an experiment is performed on a sample for which  $b_{\text{Ge}} \neq b_{\text{Se}}$ .

### 148 3. EXPERIMENTAL METHOD

#### 149 3.1. Glass Synthesis and Characterization

150 Elemental Ge (99.999 %, Alpha Aesar) and Se powders (99.999+ %, Sigma-Aldrich),  
 151 with the desired mass ratio, were loaded into a silica ampoule of 5 mm inner diameter  
 152 and 1 mm wall thickness that had been etched using a 48 wt% solution of hydrofluoric  
 153 acid, rinsed using water then acetone, and baked dry under vacuum at 800 °C for  
 154 3 h. The ampoule was loaded in a high-purity argon-filled glove box, isolated using a  
 155 Young's tap, and then transferred to a vacuum line where it was sealed under a pressure

of  $10^{-5}$  Torr. The sealed ampoule was placed in a rocking furnace, which was heated at a rate of  $2\text{ }^{\circ}\text{C min}^{-1}$  from ambient to a temperature of  $975\text{ }^{\circ}\text{C}$ , dwelling for 1 h each at temperatures of  $221\text{ }^{\circ}\text{C}$ ,  $685\text{ }^{\circ}\text{C}$  and  $938\text{ }^{\circ}\text{C}$ , i.e., near to the melting and boiling points of Se, and the melting point of Ge, respectively. The highest temperature was maintained for 47 h before the rocking motion was stopped, and the furnace was placed vertically for 1 h to let the melt collect at the bottom of the ampoule. The furnace was then cooled at a rate of  $2\text{ }^{\circ}\text{C min}^{-1}$  to a temperature  $100\text{ }^{\circ}\text{C}$  above the liquidus temperature  $T_L$  (Figure 1), where the sample was left to equilibrate for 4 h, and the ampoule was dropped into an ice/water mixture. The sample (of mass  $\sim 3.6\text{ g}$ ) was broken out of the ampoule inside an argon-filled glove box and transferred into a vanadium container of outer diameter 7 mm and wall thickness 0.1 mm ready for the diffraction experiment. Glassy samples prepared in this way showed no indication of Ge-O or Se-O impurity bands in the measured infrared transmission spectra, e.g., in the region around  $735\text{--}781\text{ cm}^{-1}$  (Savage and Nielsen 1965). A sample of glassy  $\text{GeSe}_4$ , as prepared by using an almost identical procedure but with only 10 h of rocking, was investigated by both energy dispersive x-ray spectroscopy (EDS) and Raman spectroscopy, and was found to be homogeneous on a sub-micron to centimetre length scale (Pierre Lucas, private communication).

The density of each sample was measured using a Quantachrome MICRO-ULTRAPYC 1200e pycnometer operated with helium gas. The results are compared to those obtained from other measurements in Figure 2. The comparison shows that systematically smaller densities were obtained in the work by Bhosle et al. (2012b). In the latter, agreement is claimed with the molar volume  $V_m$  values given by Mahadevan et al. (1995), but the latter were incorrectly copied from the work of Feltz et al. (1983). As shown in Figure 3, the molar volumes measured by Feltz et al. (1983) are not in quantitative agreement with the work of Bhosle et al. (2012b). Nevertheless, the data sets of Bhosle et al. (2012b), Feltz et al. (1983), Ota et al. (1978) and Yang et al. (2013) point to a minimum value of  $V_m$  in the interval  $0.20 \lesssim x \lesssim 0.25$  (Bhageria et al., 2014). The present results show a shallow minimum around  $x = 0.19(4)$  corresponding to  $V_m = 17.95(5)\text{ cm}^3\text{ mol}^{-1}$ .

The glass transition temperature  $T_g$  was measured by using a TA Instruments Q200 Differential Scanning Calorimeter operated in a TMDSC mode. Each scan comprised a temperature increasing and a temperature decreasing part, both performed at a rate of  $3\text{ }^{\circ}\text{C min}^{-1}$  and temperature modulation of  $1\text{ }^{\circ}\text{C}$  per 100 s. The maximum temperature was set to give complete coverage of the glass-transition region whilst avoiding crystallisation. The  $T_g$  values taken from the onset of the glass transition as manifested in the total heat flow measured during the temperature increasing part of a scan are plotted in Figure 4. The results are in the range of values previously reported for glasses in the  $\text{Ge}_x\text{Se}_{1-x}$  system. In addition, in order to make a like-for-like comparison with the glass transition temperatures reported by Boolchand and co-workers from TMDSC experiments (Bhosle et al., 2012a, 2012b; Boolchand 2000; Boolchand and Bresser 2000; Feng et al., 1997; Wang et al., 2005), a value  $T_{g1}$  was

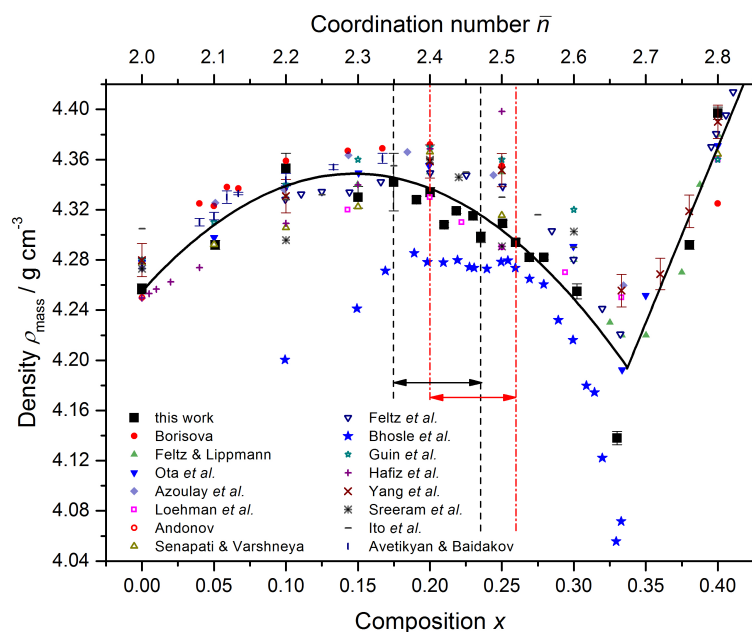


**Figure 2.** The dependence of the mass density at room temperature  $\rho_{\text{mass}}$  for the  $\text{Ge}_x\text{Se}_{1-x}$  system on the composition  $x$  and mean coordination number  $\bar{n} = 2(1+x)$ . The results from the present work at  $\approx 22^\circ\text{C}$  are compared to those taken from Andonov (1982); Avetikyan and Baidakov (1972); Azoulay et al. (1975); Bhosle et al. (2012b); Borisova (1981); Feltz et al. (1983); Feltz and Lippmann (1973); Guin et al. (2002b); Hafiz et al. (1993); Ito et al. (1988); Loehman et al. (1972); Ota et al. (1978); Senapati and Varshneya (1995); Sreeram et al. (1991b); and Yang et al. (2013). The solid (black) curves are drawn as guides for the eye. The pairs of vertical dashed (black) or chained (red) lines, and associated horizontal arrows, mark compositions for which  $\Delta H_{\text{nr}} \simeq 0$  as found in the present work or in the work of Boolchand et al. (2001a), respectively.

198 taken from the midpoint of the glass-transition region for the reversing heat-flow in  
 199 the temperature increasing part of a scan, and a value  $T_{\text{g}2}$  was also taken from the  
 200 midpoint of the glass-transition region for the reversing heat-flow in the temperature  
 201 decreasing part of a scan, and the mean value  $T_{\text{g,rev}} = (T_{\text{g}1} + T_{\text{g}2})/2$  was taken. The  
 202 results for  $T_{\text{g,rev}}$  from the present work are in agreement with those previously obtained  
 203 by Boolchand and co-workers, as shown by the inset to Figure 4.

204 The non-reversing enthalpy  $\Delta H_{\text{nr}}$  was obtained from the same TMDSC scans used  
 205 to obtain  $T_{\text{g,rev}}$  by following the procedure described by Chen et al. (2010b), which  
 206 includes a frequency correction. Independent measurements were made on several  
 207 samples from each composition that had been aged at room temperature for a minimum  
 208 of 37 days, and the mean and standard deviation were taken to find  $\Delta H_{\text{nr}}$  and its error.  
 209 The results give  $\Delta H_{\text{nr}} \simeq 0$ , which is the defining characteristic of the intermediate phase,  
 210 for the composition range  $0.175(8) \leq x \leq 0.235(8)$  (Figure 5). This composition range  
 211 compares to previously reported ‘reversibility windows’ of  $0.225 \leq x \leq 0.230$  (Feng et  
 212 al., 1997),  $0.20(1) \leq x \leq 0.26(1)$  (Boolchand et al., 2001a) or  $0.195(5) \leq x \leq 0.260(5)$

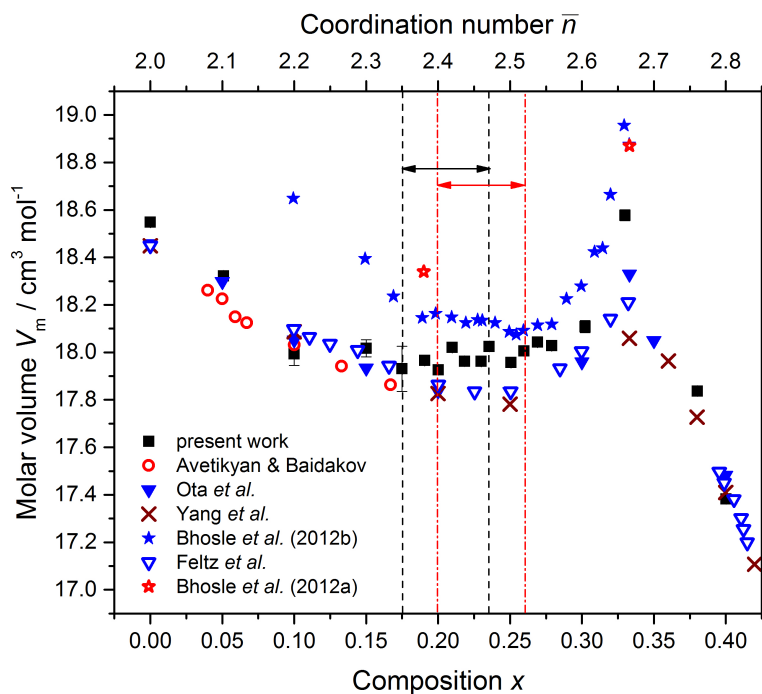


**Figure 3.** The dependence of the molar volume at room temperature  $V_m$  for the  $\text{Ge}_x\text{Se}_{1-x}$  system on the composition  $x$  and mean coordination number  $\bar{n} = 2(1+x)$ . The results from the present work are compared to those taken from Avetikyan and Baidakov (1972); Bhosle et al. (2012b); Feltz et al. (1983); Ota et al. (1978); and Yang et al. (2013). Data points are also given for the ‘dry’ samples prepared by Bhosle et al. (2012a). The pairs of vertical dashed (black) or chained (red) lines, and associated horizontal arrows, mark compositions for which  $\Delta H_{\text{nr}} \simeq 0$  as found in the present work or in the work of Boolchand et al. (2001a), respectively.

213 (Bhosle et al., 2012b) for the  $\text{Ge}_x\text{Se}_{1-x}$  system. The composition range found in the  
 214 present work is therefore shifted to lower  $x$ , and its mid-range value of  $x = 0.205(8)$   
 215 is in agreement, within the experimental error, with the expectation from mean-field  
 216 constraint-counting theory of a rigid to floppy transition in the  $\text{Ge}_x\text{Se}_{1-x}$  system at  $x$   
 217  $= 0.20$  where  $\bar{n} = 2.40$  (Thorpe 1983). The activation energy for enthalpy relaxation  
 218  $E_A$ , as measured by differential scanning calorimetry (DSC) experiments that employed  
 219 different cooling rates (Lucas et al., 2009), also shows a minimum around  $x = 0.20$   
 220 (Figure 5).

### 221 3.2. Neutron diffraction experiments

222 The neutron diffraction experiments were performed at room temperature ( $\simeq 25$  °C)  
 223 using the GEM (Hannon 2005) and SANDALS (Soper 1991) diffractometers at the  
 224 ISIS pulsed neutron source. Diffraction patterns were measured for each sample in a  
 225 vanadium container, the empty container, the empty instrument, and a vanadium rod  
 226 of diameter 8.37(1) mm for normalisation purposes. Each diffraction pattern was built

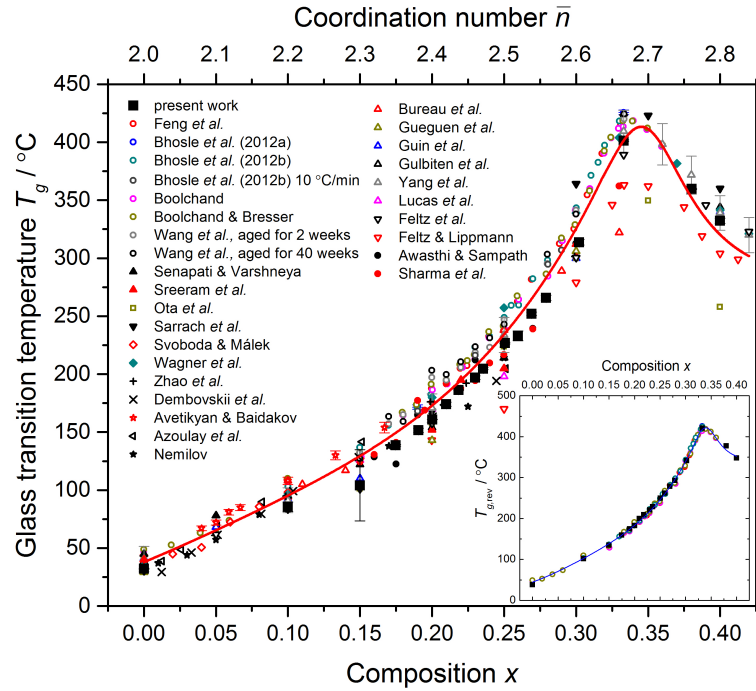


**Figure 4.** The dependence of the glass transition temperature  $T_g$  for the  $\text{Ge}_x\text{Se}_{1-x}$  system, as measured using a variety of methods, on the composition  $x$  and mean coordination number  $\bar{n} = 2(1+x)$ . The results obtained from the total heat flow in the present work are compared to the results obtained by Avetikyan and Baidakov (1972); Awasthi and Sampath (2002); Azoulay et al. (1975); Bhosle et al. (2012a, 2012b); Boolchand (2000); Boolchand and Bresser (2000); Bureau et al. (2003); Dembovskii et al., (1965); Feltz and Lippmann (1973); Feltz et al. (1983); Feng et al. (1997); Gueguen et al. (2011); Guin et al. (2002a); Gulbitten et al. (2013); Lucas et al. (2003); Nemilov (1964); Ota et al. (1978); Sarrach et al. (1976); Senapati and Varshneya (1996); Sharma et al. (2005); Sreeram et al. (1991a); Svoboda and Málek (2015); Wagner et al. (1997); Wang et al. (2005); Yang et al. (2013); and Zhao et al. (2013). The inset shows solely the results for  $T_{g,\text{rev}}$  as obtained in the present work and in the work of Boolchand and co-workers (Bhosle et al., 2012a, 2012b; Boolchand 2000, Boolchand and Bresser 2000; Feng et al., 1997; and Wang et al. 2005) – see Section 3.1 for details. The solid (red) curve in the main panel gives a least-squares fit of the measured data sets to a fourth-order polynomial at  $x \lesssim 0.32$  and to a Lorentzian function at larger  $x$  values. The solid (blue) curve in the inset gives a similar least-squares fit to the measured  $T_{g,\text{rev}}$  values.

227 up from the intensities measured for different detector groups, where these intensities  
 228 were saved at regular intervals in order to test the diffractometer stability. The data  
 229 sets were analysed detector-by-detector using the GUDRUN analysis software (Soper  
 230 2011). Inelasticity corrections were performed using the procedure described by Howe  
 231 et al. (1989). The compositions  $x = 0, 0.100, 0.150, 0.175, 0.200, 0.230, 0.251, 0.260,$   
 232  $0.279, 0.302, 0.333,$  and  $0.400$  were investigated using GEM; the compositions  $x = 0,$   
 233  $0.191, 0.210, 0.218, 0.230, 0.235,$  and  $0.269$  were investigated using SANDALS. The  
 234 uncertainty on these sample compositions  $\Delta x = \pm 0.001$ .

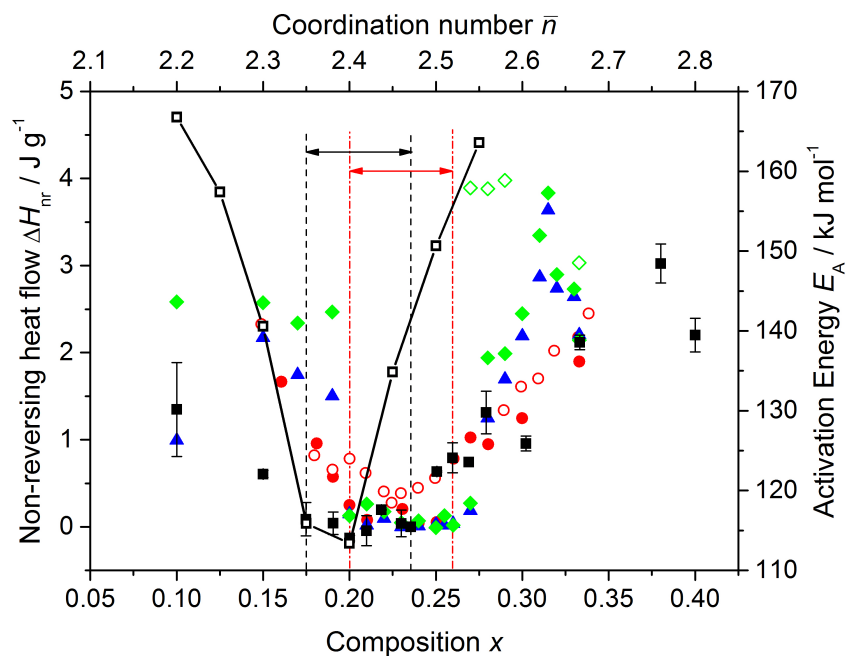


**Figure 5.** The dependence of the measured non-reversing enthalpy  $\Delta H_{nr}$  for the  $\text{Ge}_x\text{Se}_{1-x}$  system on the composition  $x$  and mean coordination number  $\bar{n} = 2(1+x)$ . The results from the present work [solid (black) squares ■ with vertical error bars] are compared to those of Feng et al. (1997) [open (red) circles ○]; Boolchand et al. (2007) [solid (red) circles ●]; and Bhosle et al. (2012b) where the samples were investigated as prepared [solid (blue) triangle ▲], after ageing for two weeks at room temperature [solid (green) diamonds ◆], or after ageing for two weeks at 240 °C [open (green) diamonds ◇]. The pairs of vertical dashed (black) or chained (red) lines, and associated horizontal arrows, mark compositions for which  $\Delta H_{nr} \simeq 0$  as found in the present work ( $0.175 \leq x \leq 0.235$ ) or in the work of Boolchand et al. (2001a) ( $0.20 \leq x \leq 0.26$ ), respectively. Also shown is the composition dependence of the activation energy for enthalpy relaxation  $E_A$  as measured in the DSC experiments of Lucas et al. (2009) [open (black) squares □].

## 235 4. NEUTRON DIFFRACTION RESULTS

### 236 4.1. Reciprocal-space properties

237 The measured total structure factors  $S(q) \simeq S_{NN}(q)$  for the  $\text{Ge}_x\text{Se}_{1-x}$  glasses are shown  
 238 in Figure 6. For the  $x = 0$  and  $x = 0.230$  compositions, that were investigated using both  
 239 GEM and SANDALS, the measured functions are in agreement within the experimental  
 240 error. For glassy Se,  $S(q)$  has a small shoulder on the low- $q$  side of the principal peak at  
 241  $q_{PP} = 1.91(2) \text{ \AA}^{-1}$ , which develops into an FSDP with increasing Ge content. The height  
 242 of the FSDP is largest at the stoichiometric composition  $x = 1/3$  where its position  
 243  $q_{\text{FSDP}} = 0.985(10) \text{ \AA}^{-1}$ . According to Fourier transform theory, a sharp peak of width  
 244  $\Delta q_i$  at a position  $q_i$  in  $S(q) \simeq S_{NN}(q)$  is associated with real-space ordering of periodicity  
 245  $2\pi/q_i$  and correlation length  $2\pi/\Delta q_i$  (Salmon 1994). Indeed, the real-space periodicity  
 246 associated with these features is directly observable for several network-forming glasses,

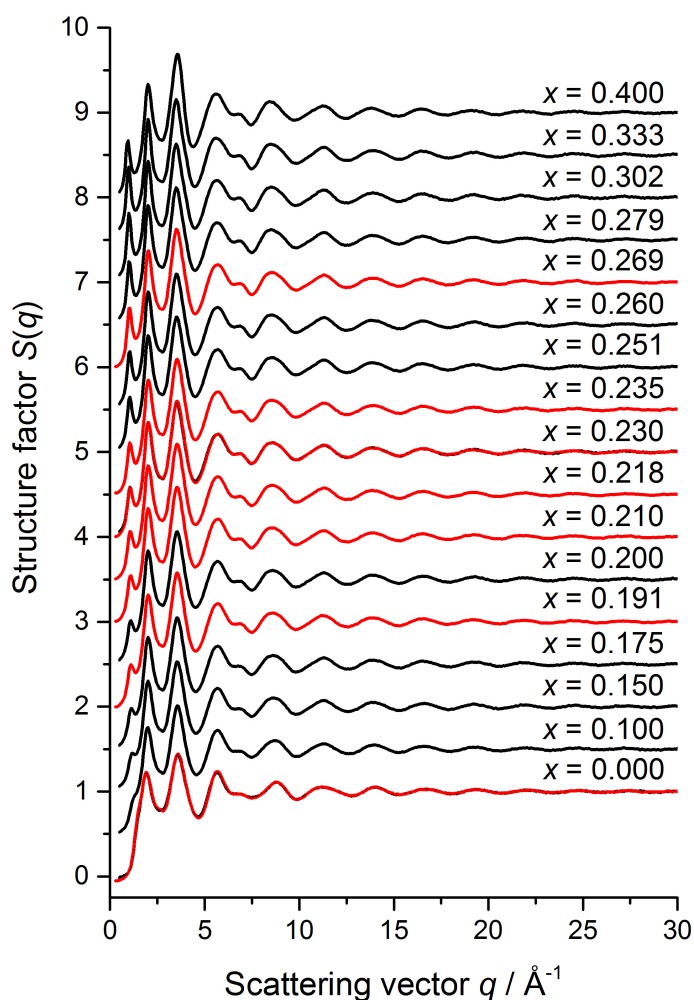


**Figure 6.** The composition dependence of the measured total structure factors  $S(q) \simeq S_{\text{NN}}(q)$  for the  $\text{Ge}_x\text{Se}_{1-x}$  system. The GEM and SANDALS data sets are shown by the solid dark (black) and solid light (red) curves with vertical error bars, respectively, where the line thickness is greater than the size of the error bars at most  $q$  values. The curves for  $x > 0$  have been displaced vertically for clarity of presentation.

247 including  $\text{Ge}_{0.333}\text{Se}_{0.667}$  (Salmon 1994, 2006; Salmon et al., 2005, 2006). The composition  
 248 dependence of the periodicity and correlation length associated with each of the first  
 249 three peaks in the measured  $S(q)$  functions is shown in Figures 7 and 8, respectively.  
 250 The full-width at half-maximum of a peak  $\Delta q_i$  was measured relative to a linear baseline  
 251 drawn between points (usually minima) deemed to mark the start and end of a peak  
 252 (Salmon 1994). The parameters obtained from the GEM and SANDALS diffractometers  
 253 are in agreement within the experimental error. The results do not show any notable  
 254 feature that can be associated specifically with an intermediate phase, although there

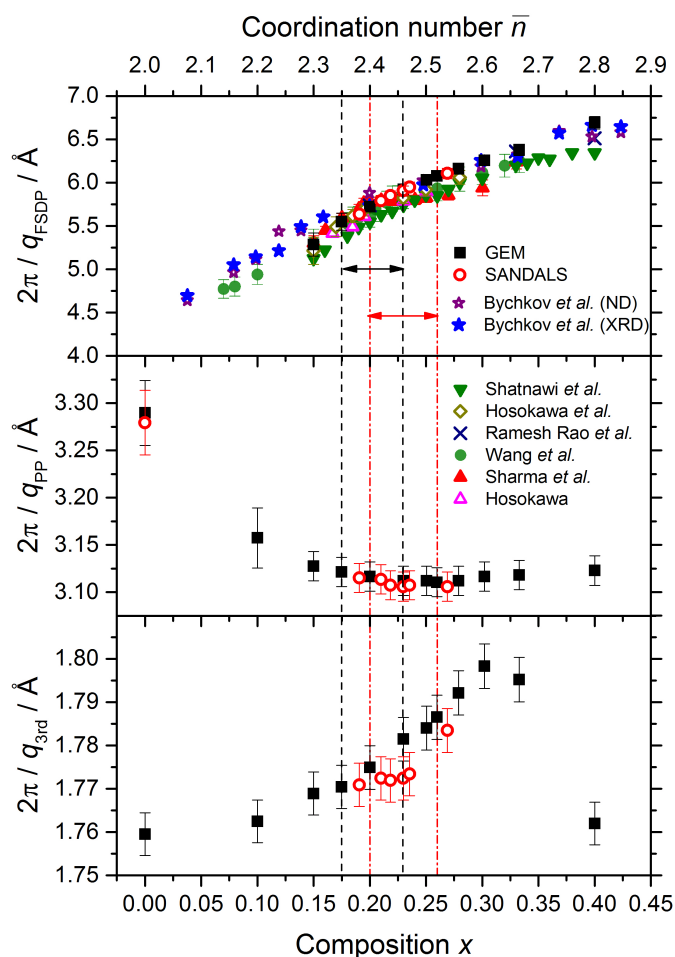


**Figure 7.** The dependence of the periodicity  $2\pi/q_i$  associated with the FSDP, principal peak (PP) and third peak in  $S(q)$  on the composition  $x$  and mean coordination number  $\bar{n} = 2(1+x)$ . The results from the present neutron diffraction (ND) work were obtained using either the GEM or SANDALS diffractometer. In the case of the FSDP, these results are compared to those obtained from the ND and high energy x-ray diffraction (XRD) work of Bychkov et al. (2005); the high energy XRD work of Shatnawi et al. (2008); the ND work of Ramesh Rao et al. (1998); the XRD work of Sharma et al. (2005) and Wang et al. (2004); and the anomalous x-ray scattering work of Hosokawa (2001) and Hosokawa et al. (2003). The pairs of vertical dashed (black) or chained (red) lines, and associated horizontal arrows, mark compositions for which  $\Delta H_{nr} \simeq 0$  as found in the present work or in the work of Boolchand et al. (2001a), respectively.

255 is a change in the correlation length associated with the FSDP at  $x \simeq 0.26$ . The  
 256 composition dependence of the periodicity  $2\pi/q_{\text{FSDP}}$  as obtained from other diffraction  
 257 experiments is also shown in Figure 7. A shoulder at  $x \simeq 0.23$ , as reported in the x-ray  
 258 diffraction work of Sharma et al. (2005), is not found in any of the other data sets.

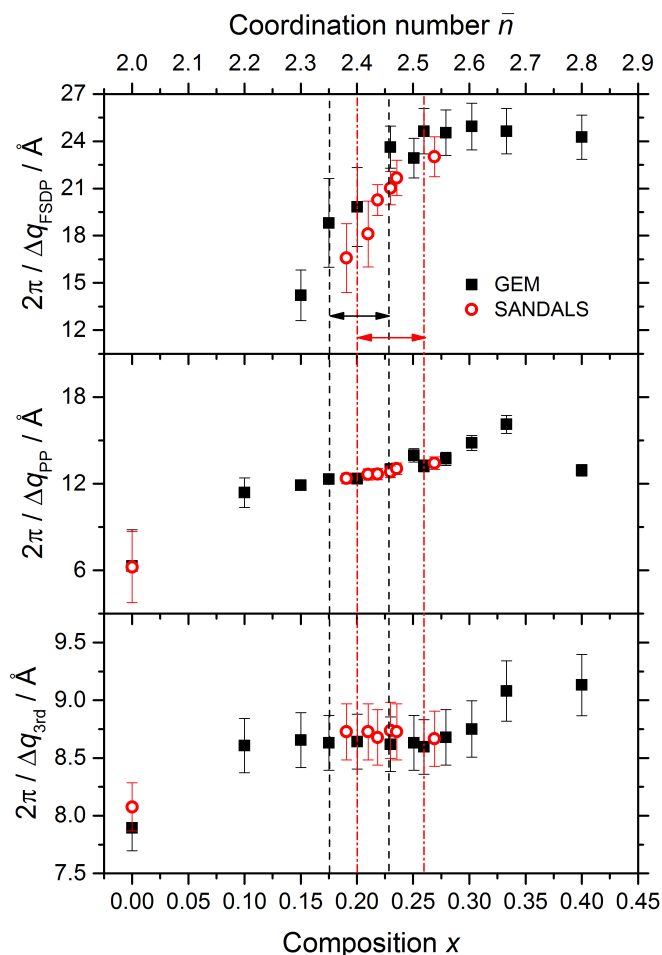


**Figure 8.** The dependence of the correlation length  $2\pi/\Delta q_i$  associated with the FSDP, principal peak (PP) and third peak in  $S(q)$  on the composition  $x$  and mean coordination number  $\bar{n} = 2(1+x)$ . The results were obtained using either the GEM or SANDALS diffractometer. The pairs of vertical dashed (black) or chained (red) lines, and associated horizontal arrows, mark compositions for which  $\Delta H_{\text{nr}} \simeq 0$  as found in the present work or in the work of Boolchand et al. (2001a), respectively.

#### 259 4.2. Real-space properties

260 The measured total pair-distribution functions  $g(r) \simeq g_{\text{NN}}(r)$  are shown in Figure 9.  
 261 The large  $q_{\text{max}}$  values accessed by the neutron diffractometers ensure that  $M(q)$  has a  
 262 minimal effect on  $S(q)$  (Eq. (2)), so the  $g(r)$  functions do not show associated Fourier  
 263 transform artifacts. The mean coordination number  $\bar{n}$  for each glass composition was  
 264 therefore obtained by direct integration of the first peak in  $g(r)$  (Eq. (3)), i.e., there  
 265 was no need to apply a fitting procedure in order to account for the effect of a finite  
 266  $q_{\text{max}}$  value (Petri et al., 2000; Salmon and Petri 2003). The composition dependence of  
 267 the measured  $\bar{n}$  values is shown in Figure 10, where the results are compared to those  
 268 obtained from the EXAFS experiments of Zhou et al. (1991) and the first-principles  
 269 molecular dynamics simulations of Inam et al. (2007). The predictions of the ‘8-N’

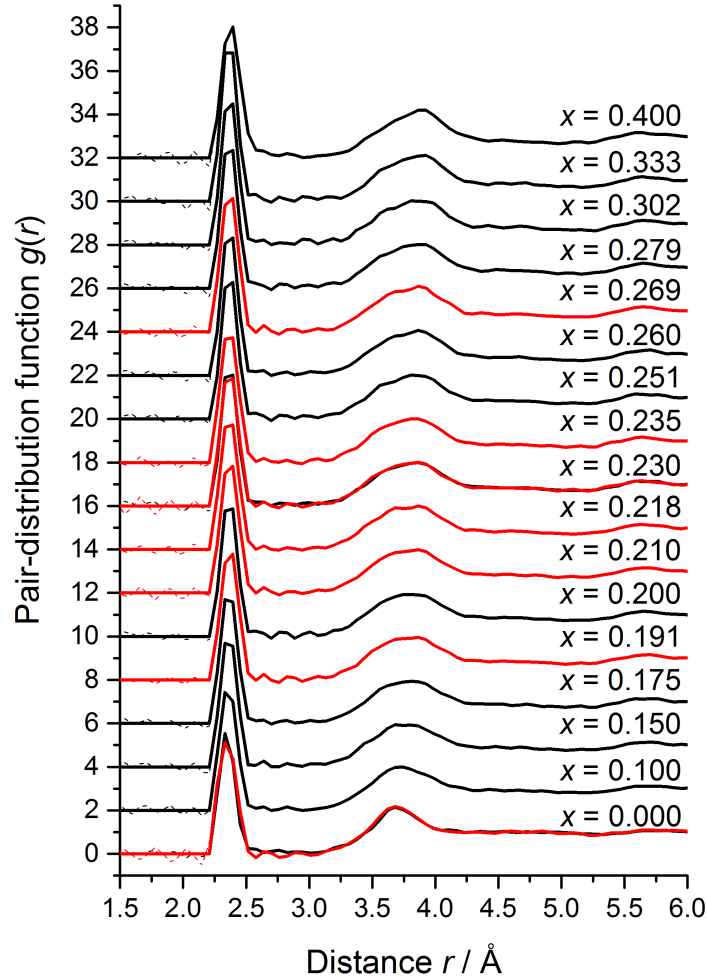


**Figure 9.** The composition dependence of the measured total pair-distribution function  $g(r) \simeq g_{\text{NN}}(r)$  for the  $\text{Ge}_x\text{Se}_{1-x}$  system, as obtained by Fourier transforming the spline fitted  $S(q)$  functions shown in Figure 6 with  $q_{\text{max}}$  set at a node in  $S(q)$  at  $\simeq 32 \text{ \AA}^{-1}$ . The GEM and SANDALS data sets are shown by the dark solid (black) and light solid (red) curves, respectively. The Fourier transform artifacts at  $r$  values smaller than the distance of closest approach between two atoms are shown by broken curves oscillating about the  $g(r \rightarrow 0) = 0$  limit. The curves for  $x > 0$  have been displaced vertically for clarity of presentation.

270 rule are also given, where the curves for the CON and RCN models take into account  
 271 the small mismatch between the coherent neutron scattering lengths of Ge and Se of  
 272 natural isotopic abundance (Section 2). The results show that  $\bar{n}$  increases monotonically  
 273 with  $x$  and, within the experimental error, the values are in accordance with the ‘8-N’  
 274 rule. They do not show any notable feature that can be associated specifically with  
 275 the intermediate phase, such as a deviation from the ‘8-N’ rule as reported by Inam et

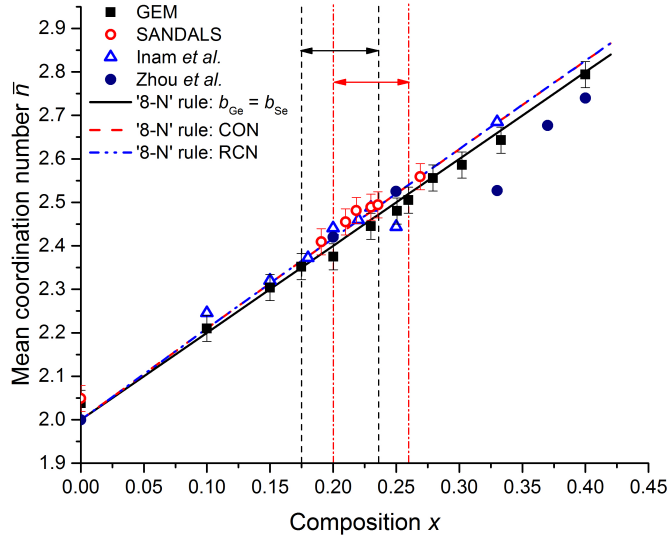


**Figure 10.** The composition dependence of the mean coordination number  $\bar{n}$  for the  $\text{Ge}_x\text{Se}_{1-x}$  system. The neutron diffraction results from GEM and SANDALS are compared to the EXAFS results of Zhou et al., (1991) and to the first-principles molecular dynamics results of Inam et al., (2007). The expectations of the ‘8-N’ rule are also given, where the curves were calculated (i) for glassy samples for which  $b_{\text{Ge}} = b_{\text{Se}}$  (see Eq. (5)), or (ii) for the expectations of the CON and RCN models, taking into account a small mismatch between the values of  $b_{\text{Ge}}$  and  $b_{\text{Se}}$  for the measured samples (see Eq. (3)). The pairs of vertical dashed (black) or chained (red) lines, and associated horizontal arrows, mark compositions for which  $\Delta H_{\text{ir}} \simeq 0$  as found in the present work or in the work of Boolchand et al. (2001a), respectively.

276 al. (2007).

## 277 5. VISCOSITY AND FRAGILITY INDEX

278 As motivated in Section 1, the composition dependence of  $\eta(T_L)$  may reveal a dynamical  
 279 signature of the intermediate phase. To investigate this possibility, the MYEGA model  
 280 (Mauro et al., 2009) for the viscosity at absolute temperature  $T$  was adopted where, for  
 281 a given composition  $x$ ,

$$282 \log_{10} \eta(T) = \log_{10} \eta_{\infty} + (12 - \log_{10} \eta_{\infty}) \frac{T_g}{T} \exp \left[ \left( \frac{m_{\text{visc}}}{12 - \log_{10} \eta_{\infty}} - 1 \right) \left( \frac{T_g}{T} - 1 \right) \right]. \quad (6)$$

283 Here,  $\log_{10} \eta_{\infty}$  is the logarithm of the high-temperature viscosity,  $T_g$  is the glass  
 284 transition temperature (in absolute units) corresponding to  $\eta(T_g) = 10^{12}$  Pa s, and  
 285  $m_{\text{visc}} \equiv d \log_{10} \eta / d(T_g/T)|_{T=T_g}$  is the fragility index. The model was used to fit the  
 286 measured viscosity data for Se (Cukierman and Uhlmann 1973; Gueguen et al., 2011;  
 287 Kořtál and Málek 2010),  $\text{Ge}_{0.10}\text{Se}_{0.90}$  (Gueguen et al., 2011; Nemilov 1964, Senapati and  
 288 Varshneya 1996),  $\text{Ge}_{0.20}\text{Se}_{0.80}$  (Gueguen et al., 2011; Nemilov 1964), and  $\text{Ge}_{0.25}\text{Se}_{0.75}$

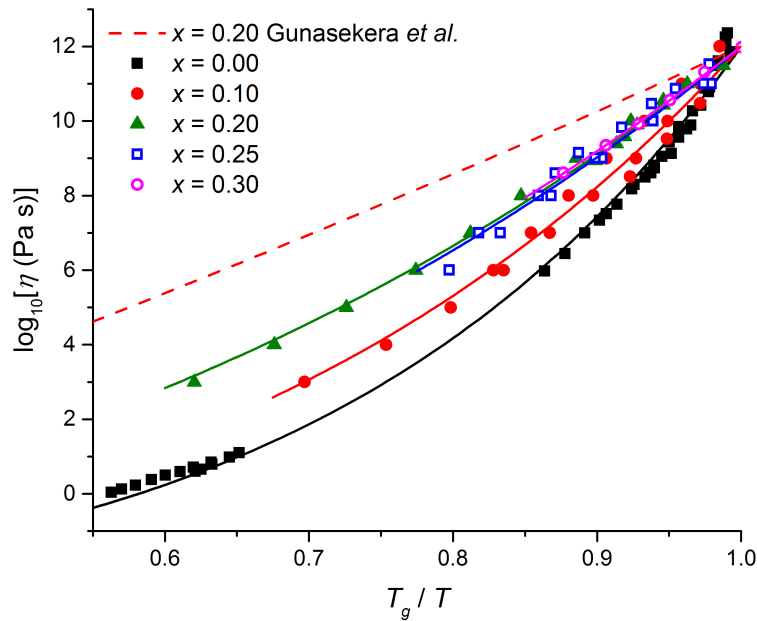


**Figure 11.** The dependence of  $\log_{10} [\eta (\text{Pa s})]$  on the ratio of absolute temperatures  $T_g/T$ . The solid curves show fits of the MYEGA model to the measured viscosity data shown by the symbols for Se (Cukierman and Uhlmann 1973; Gueguen et al., 2011; Košťál and Málek 2010),  $\text{Ge}_{0.10}\text{Se}_{0.90}$  (Gueguen et al., 2011; Nemilov 1964, Senapati and Varshneya 1996),  $\text{Ge}_{0.20}\text{Se}_{0.80}$  (Gueguen et al., 2011; Nemilov 1964),  $\text{Ge}_{0.25}\text{Se}_{0.75}$  (Gueguen et al., 2011; Nemilov 1964; Senapati and Varshneya 1996) or  $\text{Ge}_{0.30}\text{Se}_{0.70}$  (Gueguen et al., 2011), where the logarithm of the high-temperature viscosity was treated as a fixed parameter set at  $\log_{10} [\eta_{\infty} (\text{Pa s})] = -2.93$  (Zheng et al., 2011). The broken (red) curve shows the prediction at  $x = 0.20$  of the MYEGA model if the fragility index  $m_{\text{visc}}$  is equated to  $m_{\text{DSC}} = 17.7$  as found in the TMDSC measurements of Gunasekera et al. (2013) (see Figure 12).

289 (Gueguen et al., 2011; Nemilov 1964; Senapati and Varshneya 1996) where two or more  
 290 of the data sets are self-consistent, and the measured viscosity data for  $\text{Ge}_{0.30}\text{Se}_{0.70}$   
 291 (Gueguen et al., 2011) where only one data set is available. For a given composition,  
 292 the logarithm of the high-temperature viscosity was treated as either a fitting parameter  
 293 or a fixed parameter set at  $\log_{10} [\eta_{\infty} (\text{Pa s})] = -2.93$  (Zheng et al., 2011). The fits  
 294 corresponding to  $\log_{10} [\eta_{\infty} (\text{Pa s})] = -2.93$  are shown in Figure 11, and give values of  
 295  $T_g$  and  $m_{\text{visc}}$  (Figure 12) that are within the spread of values reported in the literature  
 296 from viscosity measurements (Table 1).

297 The measured data sets shown in Figure 12 give a spread in values for the  
 298 composition dependence of the fragility index. For example, a least-squares parabolic  
 299 fit to the  $m_{\text{visc}}$  values of Senapati and Varshneya (1996) leads to a minimum at  $x =$   
 300  $0.196(2)$ , whereas a similar fit to all of the  $m_{\text{visc}}$  data points leads to a minimum at  
 301  $x = 0.223(2)$ , consistent with the value  $x = 0.225$  previously reported by Stølen et

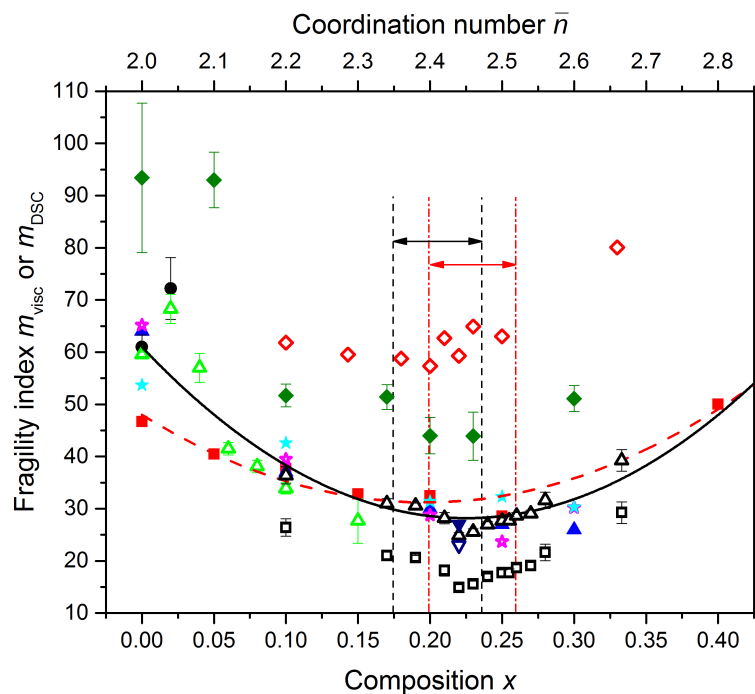


**Figure 12.** The dependence of the fragility index  $m_{\text{visc}}$  or  $m_{\text{DSC}}$  for the  $\text{Ge}_x\text{Se}_{1-x}$  system on the composition  $x$  and mean coordination number  $\bar{n} = 2(1+x)$ . The data points are from the viscosity measurements of Senapati and Varshneya (1996) [solid (red) squares  $\blacksquare$ ], Gueguen et al. (2011) [solid (blue) triangles  $\blacktriangle$ ] and Svoboda and Málek (2015) [solid (black) circles  $\bullet$ ], or from fits to viscosity data using the MYEGA model with the logarithm of the high-temperature viscosity treated as either a fitting parameter [solid (magenta) stars  $\star$ ] or a fixed parameter set at  $\log_{10}[\eta_{\infty}(\text{Pa s})] = -2.93$  [solid (cyan) stars  $\star$ ]. Least-squares parabolic fits are shown for (i) all of these viscosity derived data points [solid (black) curve], and (ii) solely the  $m_{\text{visc}}$  values of Senapati and Varshneya (1996) [broken (red) curve]. The  $m_{\text{visc}}$  values estimated from the molecular dynamics work of Yildirim et al. (2016b) are given by the open (red) diamonds  $\diamond$ . Also shown are the  $m_{\text{DSC}}$  values from Gunasekera et al. (2013) as measured [open (black) squares  $\square$ ] or after shifting by 10 units [open (black) triangles  $\triangle$ ]; Svoboda and Málek (2015) [open (green) triangles  $\triangle$ ]; Li et al. (2017) for samples prepared at  $x = 0.22$  using short and long sample reaction times of 34 h [open (blue) downward triangle  $\nabla$ ] versus 192 h [solid (blue) downward triangle  $\blacktriangledown$ ]; and Zhao et al. (2013) [solid (green) diamonds  $\blacklozenge$ ]. The pairs of vertical dashed (black) or chained (red) lines, and associated horizontal arrows, mark compositions for which  $\Delta H_{\text{nr}} \approx 0$  as found in the present work or in the work of Boolchand et al. (2001a), respectively.

302 al. (2002). The  $m_{\text{DSC}}$  values of Gunasekera et al. (2013) are smaller than other values  
 303 of the fragility index and, for several intermediate phase compositions, are even smaller  
 304 than the fragility index of silica  $m_{\text{visc}} \simeq 21$ , where the latter was obtained by applying  
 305 the MYEGA model to the viscosity data listed by Doremus (2002). A large disparity  
 306 between  $m_{\text{visc}}$  and  $m_{\text{DSC}}$  is, however, unexpected for strong glass-forming systems: the  
 307 approximation  $m_{\text{visc}} \simeq m_{\text{DSC}}$  is expected to become less accurate with increasing fragility  
 308 because of the use of an Arrhenius approximation in DSC work, where the  $m_{\text{DSC}}$  values

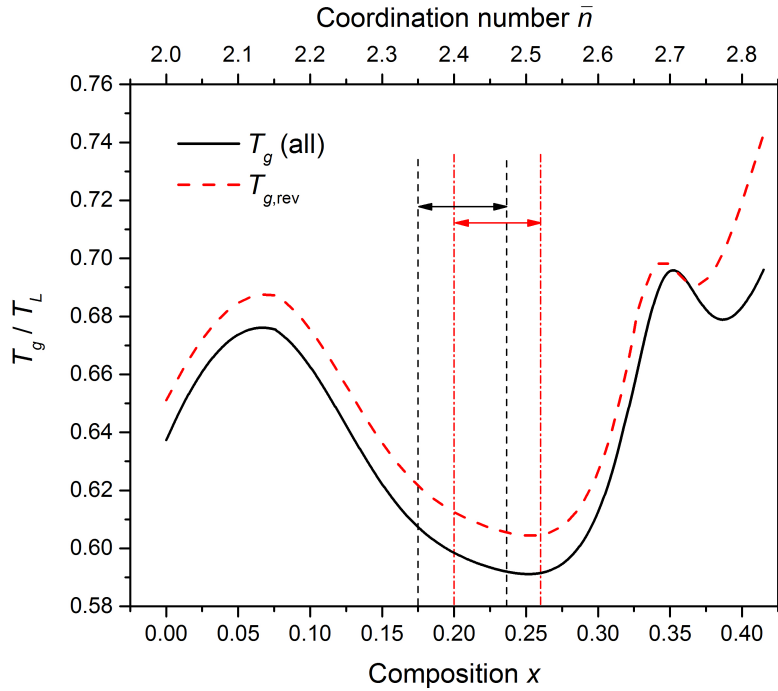


**Figure 13.** The dependence of the ratio of absolute temperatures  $T_g/T_L$  for the  $\text{Ge}_x\text{Se}_{1-x}$  system on the composition  $x$  and mean coordination number  $\bar{n} = 2(1+x)$ . The  $T_L$  values were taken from the least-squares fit to the experimental data shown in Figure 1, and the glass transition values were taken from the least-squares fit to either (i) all of the measured  $T_g$  values shown in the main panel of Figure 4, or (ii) solely the  $T_{g,\text{rev}}$  values shown in the inset to Figure 4. The resultant  $T_g/T_L$  versus  $x$  curves are shown by the solid (black) and broken (red) curves, respectively. The pairs of vertical dashed (black) or chained (red) lines, and associated horizontal arrows, mark compositions for which  $\Delta H_{\text{nr}} \simeq 0$  as found in the present work or in the work of Boolchand et al. (2001a), respectively.

309 are often smaller than their  $m_{\text{visc}}$  counterparts (Zheng et al., 2017). As discussed by  
 310 Svoboda and Málek (2015), the small  $m_{\text{DSC}}$  values of Gunasekera et al. (2013) may  
 311 originate from the exploration of a narrow range of relaxation times in their TMDSC  
 312 experiments. There may also be an issue in interpreting the imaginary part of the heat  
 313 capacity signal  $C_p''$  from TMDSC experiments, which is used to extract  $m_{\text{DSC}}$ , when it  
 314 cannot be represented by a single Gaussian function, e.g., when there are two relaxation  
 315 channels that originate from different structural motifs (Yang et al., 2012, Gulbiten  
 316 2014). A shift in the Gunasekera et al. (2013)  $m_{\text{DSC}}$  values to better match the fragility  
 317 index of glassy  $\text{Ge}_{0.10}\text{Se}_{0.90}$  found in the work by Svoboda and Málek (2015) leads to  
 318 results that are more consistent with the  $m_{\text{DSC}}$  values of 23(2)–27(2) measured for  
 319  $\text{Ge}_{0.22}\text{Se}_{0.78}$  by Li et al. (2017), and better match the measured composition dependence  
 320 of  $m_{\text{visc}}$  (Figure 12). In comparison, the  $m_{\text{DSC}}$  values of Zhao et al. (2013) are larger  
 321 than expected from the other experimental work, and take minimal values for the range  
 322  $0.22 \lesssim x \lesssim 0.23$ .

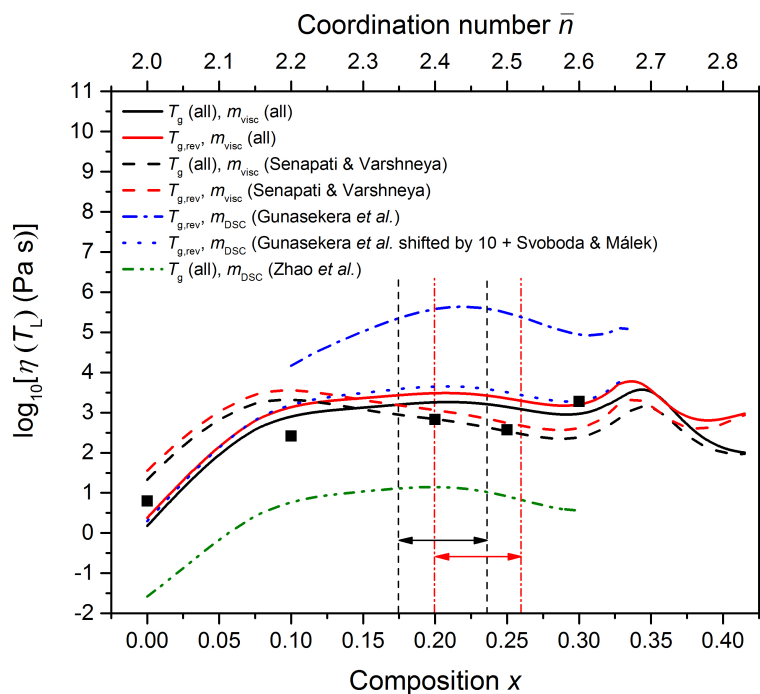


**Figure 14.** The dependence of  $\log_{10} \eta(T_L)$  for the  $\text{Ge}_x\text{Se}_{1-x}$  system, as calculated using the MYEGA model with  $\log_{10} [\eta_x (\text{Pa s})] = -2.93$ , on the composition  $x$  and mean coordination number  $\bar{n} = 2(1+x)$ . The solid (black) squares correspond to the fitted data sets shown in Figure 11 where the associated  $m_{\text{visc}}$  values are listed in Table 1. The solid (black) and solid (red) curves show the results obtained by taking  $m_{\text{visc}}$  from the solid (black) curve in Figure 12 and  $T_g/T_L$  from either the solid (black) or broken (red) curve in Figure 13, respectively. The broken (black) and broken (red) curves show the results obtained by taking  $m_{\text{visc}}$  from the broken (red) curve in Figure 12 and  $T_g/T_L$  from either the solid (black) or broken (red) curve in Figure 13, respectively. The chained (blue) and dotted (blue) curves show the results obtained by taking  $T_g/T_L$  from the broken (red) curve in Figure 13 and by assuming that  $m_{\text{visc}} \simeq m_{\text{DSC}}$ , with  $m_{\text{DSC}}$  either (i) taken from the results of Gunasekera et al. (2013) or (ii) obtained by combining the results of Svoboda and Málek (2015) with the shifted results of Gunasekera et al. (2013) (see Figure 12), respectively. The chained (green) curve shows the results obtained by taking  $T_g/T_L$  from the solid (black) curve in Figure 13 and by assuming that  $m_{\text{visc}} \simeq m_{\text{DSC}}$ , with  $m_{\text{DSC}}$  taken from the results of Zhao et al. (2013). The pairs of vertical dashed (black) or chained (red) lines, and associated horizontal arrows, mark compositions for which  $\Delta H_{\text{nr}} \simeq 0$  as found in the present work or in the work of Boolchand et al. (2001a), respectively.

323 Figure 13 shows the composition dependence of the ratio of absolute temperatures  
 324  $T_g/T_L$ , where the composition dependence of  $T_L$  was taken from a least-squares fit to the  
 325 data shown in Figure 1 and the composition dependence of  $T_g$  was taken from a least-  
 326 squares fit to the full set of data points shown in Figure 4. These  $T_g$  values originate  
 327 predominantly from DSC experiments (with a few results from dilatometry, indentation  
 328 and viscosity experiments), and were used as an approximation to the viscosity derived  
 329 values on account of the sparsity of viscosity measurements for the  $\text{Ge}_x\text{Se}_{1-x}$  system.

**Table 1.** The fragility index  $m_{\text{visc}}$  and glass transition temperature  $T_{\text{g,visc}}$  corresponding to a viscosity  $\eta(T_{\text{g,visc}}) = 10^{12}$  Pa s. The results obtained by fitting viscosity data to the MYEGA model with  $\log_{10} [\eta_{\infty} (\text{Pa s})] = -2.93$  (Figure 11) are compared to values of  $m_{\text{visc}}$  and  $T_{\text{g,visc}}$  taken from the literature. Also listed are the values of the glass transition temperature  $T_{\text{g,DSC}}$  taken from the onset of the glass transition in the total heat flow measured in the TMDSC experiments of the present work (Figure 4).

$x$	$m_{\text{visc}}$	$T_{\text{g,visc}}(^{\circ}\text{C})$	$m_{\text{visc}}$ (literature)	$T_{\text{g,visc}}$ (literature)( $^{\circ}\text{C}$ )	$T_{\text{g,DSC}}(^{\circ}\text{C})$
0	54	26	47–64 <sup>a,c,d</sup>	28–45 <sup>a,c,d</sup>	32(1)
0.10	43	89	37–38 <sup>a,c</sup>	83–95 <sup>a,b,c</sup>	86(4)
0.20	31	158	30–32 <sup>a,c</sup>	154–157 <sup>a,b,c</sup>	161(1)
0.25	32	219	27–29 <sup>a,c</sup>	214–219 <sup>a,b,c</sup>	227(1)
0.30	30	306	26 <sup>a</sup>	307 <sup>a</sup>	314(2)

<sup>a</sup> Gueguen et al. (2011); <sup>b</sup> Nemilov (1964); <sup>c</sup> Senapati and Varshneya (1996); <sup>d</sup> Svoboda and Málek (2015).

330 At compositions for which both glass transition temperatures are available (Table 1),  
 331 a discrepancy  $\lesssim 10$   $^{\circ}\text{C}$  is indicated, corresponding to a fractional uncertainty of  $\lesssim 5$  %  
 332 on the absolute values of  $T_{\text{g}}$ . In order to examine the effect on  $T_{\text{g}}/T_{\text{L}}$  of an uncertainty  
 333 on  $T_{\text{g}}$ , this ratio was also calculated after making a least-squares fit to the  $T_{\text{g,rev}}$  values  
 334 shown in the inset to Figure 4.

335 The composition dependence of  $\log_{10} \eta(T_{\text{L}})$  as predicted by the MYEGA model  
 336 with  $\log_{10} [\eta_{\infty} (\text{Pa s})] = -2.93$  is shown in Figure 14, where the ratio  $T_{\text{g}}/T_{\text{L}}$  was taken  
 337 from Figure 13 and several different scenarios were investigated for the composition  
 338 dependence of  $m_{\text{visc}}$  (Figure 12). A maximum in  $\log_{10} \eta(T_{\text{L}})$  occurs at (i)  $x = 0.21(1)$  if  
 339  $m_{\text{visc}}$  is taken from a fit to all of the viscosity derived data, or (ii)  $x = 0.21(1)$  if  $m_{\text{visc}}$   
 340 is estimated by shifting the  $m_{\text{DSC}}$  values of Gunasekera et al. (2013) and combining  
 341 them with the Svoboda and Málek (2015)  $m_{\text{DSC}}$  values. A maximum in  $\log_{10} \eta(T_{\text{L}})$   
 342 occurs at (iii)  $x = 0.22(1)$  if  $m_{\text{visc}}$  is estimated from the unshifted  $m_{\text{DSC}}$  values of  
 343 Gunasekera et al. (2013), but the calculated viscosities are several orders of magnitude  
 344 larger than expected from viscosity measurements (see also Figure 11). A maximum  
 345 in  $\log_{10} \eta(T_{\text{L}})$  occurs at (iv)  $m = 0.20(1)$  if  $m_{\text{visc}}$  is estimated from the  $m_{\text{DSC}}$  values of  
 346 Zhao et al. (2013), but in this case the calculated viscosities are significantly smaller  
 347 than expected from viscosity measurements. A maximum in  $\log_{10} \eta(T_{\text{L}})$  at  $x \sim 0.2$  is  
 348 also indicated if  $m_{\text{visc}}$  is taken from the fitted values listed in Table 1, but disappears if  
 349 the composition dependence of  $m_{\text{visc}}$  is taken from Senapati and Varshneya (1996).

350 Recently, Yildirim et al. (2016a, 2016b) used first-principles molecular dynamics  
 351 simulations to investigate the dynamics of liquid  $\text{Ge}_x\text{Se}_{1-x}$ . By applying the Stokes-  
 352 Einstein relation to the calculated Ge self-diffusion coefficients, a maximum in the  
 353 viscosity was found at  $x \simeq 0.22$  for the 777  $^{\circ}\text{C}$  isotherm, which accompanies a maximum  
 354 in the structural relaxation time for the  $\alpha$ -relaxation regime of the intermediate  
 355 scattering function at  $q = 2.1 \text{ \AA}^{-1}$ . Temperature dependent constraint counting theory,

when combined with molecular-dynamics-based constraint-counting algorithms, led to a minimum in the fragility index at this composition. A minimum in the composition dependence of the fragility index at  $x \simeq 0.2$  was also found by fitting the high-temperature viscosity data derived from first-principles molecular dynamics simulations to the MYEGA model with the logarithm of the high temperature viscosity set at  $\log_{10} [\eta_{\infty}(\text{Pa s})] = -4$  (Yildirim et al., 2016b). The majority of extracted  $m_{\text{visc}}$  values are, however, significantly larger than expected from experiment (Figure 12).

## 6. DISCUSSION

### 6.1. Glass structure and properties

As shown by the inset to Figure 4, the  $T_{\text{g,rev}}$  results of the present work are, within the experimental error, the same as those previously measured by Boolchand and co-workers. As shown in Figure 5, the composition range of the intermediate phase found in the present work,  $0.175(8) \leq x \leq 0.235(8)$ , is centred on the mean-field expectation of a floppy-to-rigid transition at  $x = 0.20$  (Thorpe 1983), and is therefore shifted to smaller  $x$  values as compared to the work of Boolchand and co-workers. As shown in Figure 2, the composition dependence of the density found in the present work is different to that reported by Bhosle et al. (2012b), and more closely matches that measured by other authors.

Bhosle et al. (2012a, 2012b) report a water-induced increase of density that accompanies a decrease in  $T_{\text{g,rev}}$  for glasses in the  $\text{Ge}_x\text{Se}_{1-x}$  system. In this way, an attempt was made to rationalise the low density values found in their work as compared to previous investigations (Figure 2). At a given composition, the density measured in the present work is also greater than reported by Bhosle et al. (2012a, 2012b), but the  $T_{\text{g,rev}}$  values are the same, e.g.,  $174(2)^\circ\text{C}$  at  $x = 0.19$  for our sample versus  $172(2)^\circ\text{C}$  at  $x = 0.19$  for the (dry) sample of Bhosle et al. (2012a). Also, the infra-red spectra for samples made using our procedure do not indicate any water contamination (Section 3.1). Hence, it is difficult to reconcile the large discrepancy in the composition dependence of the glass density between Bhosle et al. (2012b) and previous work (Figure 2) with the presence of water-contamination.

In the present work, the absence of a jump in the composition dependence of  $\Delta H_{\text{nr}}$  at the boundaries of the intermediate phase (Figure 5) might be attributed to inhomogeneous glass that originates from the allocation of insufficient time to fully react Ge and Se in the liquid state before quenching to form a glass (Bhosle et al., 2012b). However,  $\text{Ge}_x\text{Se}_{1-x}$  glasses made by using an almost identical rocking-furnace procedure show no evidence of sample heterogeneity (Section 3.1). In the work of Gunasekera et al. (2013), a small fragility index  $m_{\text{DSC}} = 14.8(5)$  for  $\text{Ge}_{0.22}\text{Se}_{0.78}$  (Figure 12) might be attributed to the preparation of homogeneous glass after a long reaction time of 144–216 h for samples of mass 2 g. However, systematically larger values of  $m_{\text{DSC}} = 23(2)$  and  $m_{\text{DSC}} = 27(2)$  are reported for  $\text{Ge}_{0.22}\text{Se}_{0.78}$  samples of similar mass ( $\sim 1.5$  g)

395 prepared using short versus long reaction times of 34 h and 192 h, respectively (Li et  
396 al., 2017).

397 The neutron diffraction results of the present work do not show any obvious  
398 structural signature of the intermediate phase. For example, they do not support a  
399 deviation from the ‘8-N’ rule as reported by Inam et al. (2007) from first-principles  
400 molecular dynamics simulations, or a shoulder in the composition dependence of  
401 the periodicity  $2\pi/q_{\text{FSDP}}$  as reported by Sharma et al. (2005) from x-ray diffraction  
402 experiments. This absence of a structural signature is consistent with the high-energy x-  
403 ray diffraction and EXAFS spectroscopy work of Shatnawi et al. (2008), who investigated  
404 samples for which  $\Delta H_{\text{nr}} \simeq 0$  for the range  $0.20 \lesssim x \lesssim 0.25$ .

405 It is conceivable that a structural signature of the intermediate phase does  
406 not manifest itself at the pair-correlation function level, as accessed by diffraction  
407 experiments (Fischer et al., 2006). Modelling methods can, however, access information  
408 on higher-body correlation functions, and Micoulaut et al. (2013) used first-principles  
409 molecular dynamics to investigate the structure of several  $\text{Ge}_x\text{Se}_{1-x}$  glasses with  
410 compositions spanning the intermediate phase. Although a compelling structural  
411 signature of the intermediate phase was not found, constraint-counting algorithms show  
412 that broken bond-bending constraints are associated with the stressed-rigid phases at  
413  $x = 1/3$  and  $x = 0.40$ . As shown by Chen et al. (2010a), the electronic structure of a  
414 glass may offer evidence of a structural origin for the intermediate phase. By combining  
415 first-principles molecular dynamics simulations with the results obtained from x-ray  
416 absorption near-edge structure (XANES) experiments made at the  $K$ -edge of both Ge  
417 and Se, it was suggested that the intermediate phase for  $\text{Ge}_x\text{Se}_{1-x}$  glasses corresponds  
418 to a composition range in which there is interplay between regions that are either Se-rich  
419 or populated by clustered  $\text{Ge}(\text{Se}_4)_{1/2}$  tetrahedra.

## 420 6.2. Comment on the utility of the intermediate phase

421 The defining feature of the intermediate phase is a composition range where  $\Delta H_{\text{nr}} \simeq 0$ .  
422 The physical interpretation of this parameter is debated (Schawe 1995; Reading 1997),  
423 with Boolchand and co-workers attributing it to the enthalpy of relaxation at  $T_g$  (Bhosle  
424 et al., 2012a). It is conjectured that glasses within the intermediate phase are stable  
425 in the sense that, for different ageing times at room temperature, there is no alteration  
426 to the total enthalpy change  $\Delta H_{\text{tot}} = \Delta H_{\text{r}} + \Delta H_{\text{nr}}$  across the glass transition: the  
427 reversing part  $\Delta H_{\text{r}}$  does not alter and, unlike the floppy and stressed-rigid phases, the  
428 non-reversing part  $\Delta H_{\text{nr}}$  remains vanishingly small (Boolchand et al., 2002; Bhosle et  
429 al., 2012b).

430 By contrast, the change in specific heat capacity  $C_p$  across the glass transition, as  
431 determined from the total enthalpy change measured in DSC experiments, has been  
432 used to monitor the effect on  $\text{Ge}_{0.10}\text{Se}_{0.90}$  and  $\text{Ge}_{0.20}\text{Se}_{0.80}$  glass fibres of ageing at  
433 room temperature for periods of up to 58 months (King 2011). The results show that  
434 glasses within the intermediate phase do relax, although the magnitude of change is

markedly smaller for  $x = 0.20$  as compared to  $x = 0.10$ . Some of this difference in response may originate from a difference in fictive temperatures: The glass fibres were quenched quickly from the melt and correspond to a high fictive temperature, whereas the samples of e.g., Bhosle et al. (2012b) were temperature cycled above  $T_g$  during a TMDSC experiment before ageing at room temperature, and therefore correspond to a low fictive temperature. Some of this difference in response may also originate from the size of the interval between  $T_g$  and the annealing temperature  $T_a$ , where the former increases with  $x$  (Figure 4). Zhao et al. (2013) looked at this issue by employing DSC to monitor the change in total enthalpy for bulk samples of melt-quenched glassy  $\text{Ge}_x\text{Se}_{1-x}$  ( $0 \leq x \leq 0.23$ ) annealed for 1 h at  $T_g$ . The samples were subsequently aged for different durations of time with  $T_a$  set at a fixed interval below  $T_g$ . All of the samples showed the same ageing characteristics, including those associated with intermediate phase compositions, with an ageing rate and kinetics that depend on the interval  $T_g - T_a$ . A Raman spectroscopy investigation of  $\text{Ge}_{0.20}\text{Se}_{0.80}$ , in which a glass equilibrated at  $T_g = 160^\circ\text{C}$  was subsequently aged at  $120^\circ\text{C}$  for a time period ranging from 6 to 240 h, showed structural relaxation with a characteristic timescale of  $\sim 40$  h during which there is a conversion from edge-sharing to corner-sharing  $\text{Ge}(\text{Se}_4)_{1/2}$  tetrahedral units (Edwards and Sen 2011). A conversion from edge-sharing to corner-sharing tetrahedral units was also observed by King (2011) in her Raman spectroscopy work on the ageing of  $\text{Ge}_{0.10}\text{Se}_{0.90}$  and  $\text{Ge}_{0.20}\text{Se}_{0.80}$  glass fibres at room temperature.

Recently,  $m_{\text{DSC}}$  values smaller than the fragility index of silica have been reported for glasses within the intermediate phase window, leading to the notion of ‘super-strong’ liquids (Gunasekera et al., 2013). This feature has been attributed to a slow homogenization of the melt when  $\text{Ge}_x\text{Se}_{1-x}$  glasses are prepared via a heating procedure in which elemental Ge and Se pieces are melted in a stationary vertically-mounted silica-ampoule, i.e., when a rocking furnace is not employed (Gunasekera et al., 2013; Bhageria et al., 2014). However, as discussed in Section 5, the numerical values for  $m_{\text{DSC}}$  reported by Gunasekera et al. (2013) lead to a temperature dependence of the viscosity that is notably different to that expected from viscosity measurements (Figure 11), leading to  $\log_{10} \eta(T_L)$  values that are significantly larger than expected (Figure 14).

Lastly, it would be helpful if advocates of the intermediate phase could develop a method for predicting its occurrence and composition range for different classes of network glass-forming systems, and the concomitant effect on the material properties. For example,  $\text{Ge}_x\text{Se}_{1-x}$  and  $\text{As}_x\text{Se}_{1-x}$  are prototypical chalcogenide glass-forming systems that feature different network topologies. In the case of  $\text{Ge}_x\text{Se}_{1-x}$ , the intermediate phase window incorporates the composition  $x = 0.20$  for which a rigid to floppy transition is expected on the basis of mean-field constraint counting theory, a minimum in the molar volume is reported for the intermediate phase window (Bhosle et al., 2012b, Bhageria et al., 2014), and the fragility index takes a minimum within this window at around  $x = 0.22$  (Section 5). In the case of  $\text{As}_x\text{Se}_{1-x}$ , however, the intermediate phase window of  $0.291(1) \leq x \leq 0.37(1)$  (Georgiev et al., 2000) or  $0.20 < x < 0.37$  (Ravindren et al., 2014) does not incorporate the mean-field

477 composition of  $x = 0.40$  for a floppy to rigid transition, a minimum in the molar volume  
478 may (Ravindren et al., 2014) or may not occur within this composition range (e.g., Feltz  
479 et al. 1983 report a minimum at  $x = 0.40$ ), and a minimum in the fragility index  $m_{\text{visc}}$   
480 occurs at  $x \simeq 0.27$  (Musgraves et al., 2011).

## 481 7. CONCLUSIONS

482 The structure of vitreous  $\text{Ge}_x\text{Se}_{1-x}$  across the glass-forming region was measured by  
483 using neutron diffraction. No clear-cut evidence could be found for a structural  
484 origin of the intermediate phase, which extends over the composition range  $0.175(8) \leq$   
485  $x \leq 0.235(8)$  as found from the non-reversing enthalpy measured using TMDSC. The  
486 dynamical properties of the  $\text{Ge}_x\text{Se}_{1-x}$  system were also probed by using the MYEGA  
487 model for the viscosity. Much of the available evidence points to a minimum in the  
488 fragility index, and a maximum in the viscosity at the liquidus temperature, that occur  
489 in the range  $0.20 \leq x \leq 0.22$ . This range incorporates the composition  $x = 0.20$  at  
490 which a floppy-to-rigid transition is expected from mean-field constraint-counting theory,  
491 in contrast to the  $\text{As}_x\text{Se}_{1-x}$  system where a minimum in the fragility index occurs at  
492  $x \simeq 0.27$  but a floppy-to-rigid transition is expected from mean-field constraint-counting  
493 theory at  $x = 0.40$ . In order to establish the extent to which these findings are related  
494 to the expectations of mean-field constraint-counting theory, or to a special range of  
495 compositions associated with the intermediate phase, it would be beneficial to make a  
496 systematic and more complete investigation on the composition dependence of  $\eta(T)$  for  
497 the  $\text{Ge}_x\text{Se}_{1-x}$  and other chalcogenide network glass-forming systems.

## 498 CONFLICT OF INTEREST STATEMENT

499 The authors declare that the research was conducted in the absence of any commercial  
500 or financial relationships that could be construed as a potential conflict of interest.

## 501 AUTHOR CONTRIBUTIONS

502 PSS and AZ designed the research; all authors contributed to the neutron diffraction  
503 experiments; AZ and KJP performed the TMDSC experiments; AZ and PSS analysed  
504 data; PSS wrote the paper.

## 505 FUNDING

506 The Bath group received support from the EPSRC via Grant Nos. EP/G008795/1 and  
507 EP/J009741/1. AZ and PSS are grateful to Corning Inc. for the award of Gordon  
508 S. Fulcher Distinguished Scholarships, during which this work was completed. AZ is  
509 supported by a Royal Society–EPSRC Dorothy Hodgkin Research Fellowship.

**ACKNOWLEDGMENTS**

We thank Kamil Wezka for help with some of the diffraction work; Punit Boolchand for advice on using the TMDSC method, and for pointing out the correct reference (Mahadevan et al. 1995) for some of the density data reported in Bhosle et al. (2012b); Pierre Lucas for access to his unpublished results on the homogeneity of chalcogenide glasses prepared by rocking-furnace methods; John Mauro, Doug Allan and Ozgur Gulbiten for helpful discussions about the MYEGA equation and calorimetry; and Tanguy Rouxel for providing the numerical data sets from Gueguen et al. (2011).

**DATA ACCESS STATEMENT**

The data sets created during this research are openly available from the University of Bath data archive at [LINK TO BE PROVIDED](#).

**REFERENCES**

- Andonov, P. (1982). Studies of non-crystalline forms of selenium. *J. Non-Cryst. Solids* 47, 297–339.
- Avetikyan, G. B., and Baidakov, L. A. (1972). Temperature dependence of the density of selenium-enriched glasses of the system Ge-Se and their thermal expansion. *Neorg. Mater.* 8, 1489–1490.
- Awasthi, A. M., and Sampath, S. (2002). Thermo-kinetic anomalies across rigidity threshold in  $\text{Ge}_x\text{Se}_{1-x}$ . *Mater. Trans.* 43, 2046–2049.
- Azoulay, R., Thibierge, H., and Brenac, A. (1975). Devitrification characteristics of  $\text{Ge}_x\text{Se}_{1-x}$  glasses. *J. Non-Cryst. Solids* 18, 33–53.
- Berkes, J. S., and Myers, M. B. (1971). Phase relations and liquid structure in the system As-Sb<sub>2</sub>Se<sub>3</sub>-Se. *J. Electrochem. Soc.* 118, 1485–1491.
- Bhageria, R., Gunasekera, K., Boolchand, P., and Micoulaut, M. (2014). Fragility and molar volumes of non-stoichiometric chalcogenides: The crucial role of melt/glass homogenization. *Phys. Status Solidi* 251, 1322–1329.
- Bhatia, A. B., and Thornton, D. E. (1970). Structural aspects of the electrical resistivity of binary alloys. *Phys. Rev. B* 2, 3004–3012.
- Bhosle, S., Gunasekera K., Boolchand, P., and Micoulaut, M. (2012a). Melt homogenization and self-organization in chalcogenides-Part I *Int. J. Appl. Glass Sci.* 3, 189–204.
- Bhosle, S., Gunasekera K., Boolchand, P., and Micoulaut, M. (2012b). Melt homogenization and self-organization in chalcogenides - part II. *Int. J. Appl. Glass Sci.* 3, 205–220.
- Boolchand, P. (2000). The maximum in glass transition temperature ( $T_g$ ) near  $x = 1/3$  in  $\text{Ge}_x\text{Se}_{1-x}$  glasses. *Asian J. Phys.* 9, 709–721.
- Boolchand, P., and Bresser, W. J. (2000). The structural origin of broken chemical order in  $\text{GeSe}_2$  glass. *Phil. Mag. B* 80, 1757–1772.
- Boolchand, P., Chen, P., Jin, M., Goodman, B., and Bresser, W. J. (2007). <sup>129</sup>I and <sup>119</sup>Sn Mössbauer spectroscopy, reversibility window and nanoscale phase separation in binary  $\text{Ge}_x\text{Se}_{1-x}$  glasses. *Physica B* 389, 18–28.
- Boolchand, P., Feng, X., and Bresser, W. J. (2001a). Rigidity transitions in binary Ge-Se glasses and the intermediate phase. *J. Non-Cryst. Solids* 293-295, 348–356.
- Boolchand, P., Georgiev, D. G., and Goodman, B. (2001b). Discovery of the intermediate phase in chalcogenide glasses. *J. Optoelectron. Adv. Mater.* 3, 703–720.
- Boolchand, P., Georgiev, D. G., Micoulaut, M. (2002). Nature of glass transition in chalcogenides. *J. Optoelectron. Adv. Mater.* 4, 823–836.

- 553 Borisova, Z. U. (1981). *Glassy Semiconductors*. New York: Springer.
- 554 Bychkov, E., Benmore, C. J., and Price, D. L. (2005). Compositional changes of the first sharp  
555 diffraction peak in binary selenide glasses. *Phys. Rev. B* 72, 172107.
- 556 Bureau, B., Troles, J., Le Floch M., Guénot, P., Smektala, F., and Lucas, J. (2003). Germanium  
557 selenide glass structures studied by  $^{77}\text{Se}$  solid state NMR and mass spectroscopy. *J. Non-Cryst.*  
558 *Solids* 319, 145–153.
- 559 Chen, P., Inam, F., and Drabold, D. A. (2010a). Structural origin of the intermediate phase in Ge-Se  
560 glasses. *Appl. Phys. Lett.* 97, 131901.
- 561 Chen, P., Boolchand, P., and Georgiev, D. G. (2010b). Long term aging of selenide glasses: Evidence  
562 of sub- $T_g$  endotherms and pre- $T_g$  exotherms. *J. Phys.: Condens. Matter* 22, 065104.
- 563 Cukierman, M., and Uhlmann, D. R. (1973). Viscous flow behaviour of selenium. *J. Non-Cryst. Solids*  
564 12, 199–206.
- 565 Cusack, N. E. (1987). *The Physics of Structurally Disordered Matter*. Bristol: Hilger.
- 566 Dembovskii, S. A., Vinogradova, G. Z., and Pashinkin, A. S. (1965). Crystallisation of glasses of the  
567 Ge-Se system. *Russ. J. Inorg. Chem.* 10, 903–905.
- 568 Doremus, R. H. (2002). Viscosity of silica. *J. Appl. Phys.* 92, 7619–7629.
- 569 Edwards, T.G., and Sen, S. (2011). Structure and relaxation in germanium selenide glasses and  
570 supercooled liquids: A Raman spectroscopic study. *J. Phys. Chem. B* 115, 4307–4314.
- 571 Elliott, S. R. (1990). *Physics of Amorphous Materials*. 2nd edn. Harlow, Longman.
- 572 Feltz, A. (1993). *Amorphous Inorganic Materials and Glasses*. Weinheim, VCH.
- 573 Feltz, A., Aust, H., and Blayer, A. (1983). Glass formation and properties of chalcogenide systems  
574 XXVI: Permittivity and the structure of glasses  $\text{As}_x\text{Se}_{1-x}$  and  $\text{Ge}_x\text{Se}_{1-x}$ . *J. Non-Cryst. Solids* 55,  
575 179–190.
- 576 Feltz, A., and Lippmann, F.-J. (1973). Zur Glasbildung im System Germanium-Selen. *Z. Anorg. Allg.*  
577 *Chem.* 398, 157–166.
- 578 Feng, X., Bresser, W. J., and Boolchand, P. (1997). Direct evidence for stiffness threshold in  
579 chalcogenide glasses. *Phys. Rev. Lett.* 78, 4422–4425.
- 580 Fischer, H. E., Barnes, A. C., and Salmon, P. S. (2006). Neutron and x-ray diffraction studies of liquids  
581 and glasses. *Rep. Prog. Phys.* 69, 233–299.
- 582 Georgiev, D. G., Boolchand, P., and Micoulaut, M. (2000). Rigidity transition and molecular structure  
583 of  $\text{As}_x\text{Se}_{1-x}$  glasses. *Phys. Rev. B* 62, R9228–R9231.
- 584 Gueguen, Y., Rouxel, T., Gadaud, P., Bernard, C., Keryvin, V., and Sangleboeuf, J.-C. (2011). High-  
585 temperature elasticity and viscosity of  $\text{Ge}_x\text{Se}_{1-x}$  glasses in the transition range. *Phys. Rev. B* 84,  
586 064201.
- 587 Guin, J.-P., Rouxel, T., Keryvin, V., Sangleboeuf, J.-C., Serre, I., and Lucas, J. (2002a). Indentation  
588 creep of Ge-Se chalcogenide glasses below  $T_g$ : Elastic recovery and non-Newtonian flow. *J. Non-*  
589 *Cryst. Solids* 298, 260–269.
- 590 Guin, J.-P., Rouxel, T., Sangleboeuf, J.-C., Melscoët, I., and Lucas, J. (2002b). Hardness, toughness,  
591 and scratchability of germanium-selenium chalcogenide glasses. *J. Am. Ceram. Soc.* 85, 1545–1552.
- 592 Gulbitten, O. (2014). An investigation of dynamic processes in selenium based chalcogenide glasses.  
593 PhD Thesis, University of Arizona.
- 594 Gulbitten, O., Mauro, J. C., and Lucas, P. (2013). Relaxation of enthalpy fluctuations during sub- $T_g$   
595 annealing of glassy selenium. *J. Chem. Phys.* 138, 244504.
- 596 Gunasekera, K., Bhosle, S., Boolchand, P., and Micoulaut, M. (2013). Superstrong nature of covalently  
597 bonded glass-forming liquids at select compositions. *J. Chem. Phys.* 139, 164511.
- 598 Hafiz, M. M., Hammad, F. H., and El-Kabany, N. A. (1993). Short- and medium-range order in Se-Ge  
599 glassy systems (I) Effect of composition. *Physica B* 183, 392–398.
- 600 Hannon, A. C. (2005). Results on disordered materials from the GEneral Materials diffractometer,  
601 GEM, at ISIS. *Nucl. Instrum. Methods Phys. Res. A* 551, 88–107.
- 602 Hosokawa, S. (2001). Atomic and electronic structures of glassy  $\text{Ge}_x\text{Se}_{1-x}$  around the stiffness threshold  
603 composition. *J. Optoelectron. Adv. Mater.* 3, 199–214.

- 604 Hosokawa, S., Oh, I., Sakurai, M., Pilgrim, W.-C., Boudet, N., Bézar, J.-F., and Kohara, S.  
605 (2011). Anomalous x-ray scattering study of  $\text{Ge}_x\text{Se}_{1-x}$  glassy alloys across the stiffness transition  
606 composition. *Phys. Rev. B* 84, 014201.
- 607 Hosokawa, S., Wang, Y., Bézar, J.-F., Sakurai, M., and Pilgrim, W.-C. (2003). Anomalous x-ray  
608 scattering studies on glassy  $\text{Ge}_x\text{Se}_{1-x}$  over a wide concentration range including the stiffness  
609 transition composition. *J. Non-Cryst. Solids* 326-327, 394–398.
- 610 Howe, M. A., McGreevy, R. L., and Howells, W. S. (1989). The analysis of liquid structure data from  
611 time-of-flight neutron diffractometry. *J. Phys.: Condens. Matter* 1, 3433–3451.
- 612 Inam, F., Shatnawi, M. T., Tafen, D., Billinge, S. J. L., Chen, P., and Drabold, D. A. (2007). An  
613 intermediate phase in  $\text{Ge}_x\text{Se}_{1-x}$  glasses: Experiment and simulation. *J. Phys.: Condens. Matter*  
614 19, 455206.
- 615 Ipsier, H., Gambino, M., and Schuster, W. (1982). The germanium-selenium phase diagram. *Monatshefte*  
616 *Chemie* 113, 389–398.
- 617 Ito, Y., Kashida, S., and Murase, K. (1988). Elastic constants of the chalcogenide glasses ( $\text{Ge}_x\text{Se}_{1-x}$ ,  
618  $\text{As}_y\text{Se}_{1-y}$  and  $\text{Ge}_{2/3z}\text{As}_{1/3z}\text{Se}_{1-z}$ ). *Solid State Comm.* 65, 449-452.
- 619 Johnson, R. W., Susman, S., McMillan J., and Volin, K. J. (1986). Preparation and characterization of  
620  $\text{Si}_x\text{Se}_{1-x}$  glasses and determination of the equilibrium phase diagram. *Mater. Res. Bull.* 21, 41–47.
- 621 King, E. A. (2011). Structure and relaxation in germanium selenide and arsenic selenide glasses. PhD  
622 Thesis, University of Arizona.
- 623 Košťál, P., and Málek, J. (2010). Viscosity of selenium melt. *J. Non-Cryst. Solids* 356, 2803–2806.
- 624 Li, P., Zhang, Y., Chen, Z., Gao, P., Wu, T., Wang, L.-M. (2017). Relaxation dynamics in the strong  
625 chalcogenide glass-former of  $\text{Ge}_{22}\text{Se}_{78}$ . *Sci. Rep.* 7, 40547.
- 626 Loehman, R. E., Armstrong, A. J., Firestone, D. W., and Gould, R. W. (1972). Composition and  
627 physical properties of amorphous bulk and thin film materials in the system Ge-Se-Te-As. *J. Non-*  
628 *Cryst. Solids* 8-10, 72–77.
- 629 Lucas, P., Doraiswamy, A., and King, E. A. (2003). Photoinduced structural relaxation in chalcogenide  
630 glasses. *J. Non-Cryst. Solids* 332, 35–42.
- 631 Lucas, P., King, E. A., Gulbiten, O., Yarger, J. L., Soignard, E., and Bureau, B. (2009). Bimodal phase  
632 percolation model for the structure of Ge-Se glasses and the existence of the intermediate phase.  
633 *Phys. Rev. B* 80, 214114.
- 634 Mahadevan, S., Giridhar, A., and Singh, A. K. (1995). Chemical ordering and topological effects in  
635 chalcogenide glass systems. *Ind. J. Pure Appl. Phys.* 33, 643–652.
- 636 Massobrio, C., Celino, M., Salmon, P. S., Martin, R. A., Micoulaut, M., and Pasquarello, A. (2009).  
637 Atomic structure of the two intermediate phase glasses  $\text{SiSe}_4$  and  $\text{GeSe}_4$ . *Phys. Rev. B* 79, 174201.
- 638 Mauro, J. C., Yue, Y., Ellison, A. J., Gupta, P. K., and Allan, D. C. (2009). Viscosity of glass-forming  
639 liquids. *Proc. Natl. Acad. Sci. USA* 106, 19780–19784.
- 640 Micoulaut, M., Kachmar, A., Bauchy, M., Le Roux, S., Massobrio, C., and Boero, M. (2013). Structure,  
641 topology, rings, and vibrational and electronic properties of  $\text{Ge}_x\text{Se}_{1-x}$  glasses across the rigidity  
642 transition: A numerical study. *Phys. Rev. B* 88, 054203.
- 643 Mikolaichuk, A. G., and Moroz, V. N. (1986). Chemical interaction and glass formation in the system  
644  $\text{Ag}_8\text{GeSe}_6\text{-GeSe-GeSe}_2$ . *Fizika Khimiiia Stekla* 12, 717–719.
- 645 Morgant, G., and Legendre, B. (1986). Etude du systeme binaire selenium-tellure. *J. Thermal Anal.*  
646 31, 377–385.
- 647 Musgraves, J. D., Wachtel, P., Novak, S., Wilkinson, J., and Richardson, K. (2011). Composition  
648 dependence of the viscosity and other physical properties in the arsenic selenide glass system. *J.*  
649 *Appl. Phys.* 110, 063503.
- 650 Nemilov, S. V. (1964). Viscosity and structure of glass system Se-Ge. *Zh. Prikl. Khim.* 37, 1020–1024.
- 651 Ota, R., and Kunugi, M. (1973). Thermal expansion coefficient and glass transition temperature for  
652 As-Se glasses. *J. Ceramic Association Japan* 81, 228–231.
- 653 Ota, R., Yamate, T., Soga, N., and Kunugi, M. (1978). Elastic properties of Ge-Se glass under pressure.  
654 *J. Non-Cryst. Solids* 29, 67–76.

- 655 Petri, I., Salmon, P. S., and Howells, W. S. (1999). Change in the topology of the glass forming liquid  
656 GeSe<sub>2</sub> with increasing temperature. *J. Phys.: Condens. Matter* 11, 10219–10227.
- 657 Petri, I., Salmon, P. S., and Fischer, H. E. (2000). Defects in a disordered world: The structure of  
658 glassy GeSe<sub>2</sub>. *Phys. Rev. Lett.* 84, 2413–2416.
- 659 Phillips, J. C. (1979). Topology of covalent non-crystalline solids I: Short-range order in chalcogenide  
660 alloys. *J. Non-Cryst. Solids* 34, 153–181.
- 661 Quenez, P., and Khodadad, P. (1969). Étude du système GeSe<sub>2</sub>-CdSe. Identification du composé  
662 Cd<sub>4</sub>GeSe<sub>6</sub>. *C. R. Acad. Sci. Paris C*, 268, 2294–2297.
- 663 Ramesh Rao, N., Krishna, P. S. R., Basu, S., Dasannacharya, B. A., Sangunni, K. S., and Gopal, E. S.  
664 R. (1998). Structural correlations in Ge<sub>x</sub>Se<sub>1-x</sub> glasses – a neutron diffraction study. *J. Non-Cryst.*  
665 *Solids* 240, 221–231.
- 666 Ravindren, S., Gunasekera, K., Tucker, Z., Diebold, A., Boolchand, P., and Micoulaut, M. (2014).  
667 Crucial effect of melt homogenization on the fragility of non-stoichiometric chalcogenides. *J. Chem.*  
668 *Phys.* 140, 134501.
- 669 Reading, M. (1997). Comments on “A comparison of different evaluation methods in modulated-  
670 temperature DSC.” *Thermochimica Acta* 292, 179–187.
- 671 Ross, L., and Bourgon, M. (1969). The germanium-selenium phase diagram. *Can. J. Chem.* 47, 2555–  
672 2559.
- 673 Salmon, P. S. (1992). The structure of molten and glassy 2:1 binary systems: An approach using the  
674 Bhatia-Thornton formalism. *Proc. R. Soc. Lond. A* 437, 591–606.
- 675 Salmon, P. S. (1994). Real space manifestation of the first sharp diffraction peak in the structure factor  
676 of liquid and glassy materials. *Proc. R. Soc. Lond. A* 445, 351–365.
- 677 Salmon, P. S. (2006). Decay of the pair correlations and small-angle scattering for binary liquids and  
678 glasses. *J. Phys.: Condens. Matter* 18, 11443–11469.
- 679 Salmon, P. S. (2007a). Structure of liquids and glasses in the Ge-Se binary system. *J. Non-Cryst. Solids*  
680 353, 2959–2974.
- 681 Salmon, P. S. (2007b). The structure of tetrahedral network glass forming systems at intermediate and  
682 extended length scales. *J. Phys.: Condens. Matter* 19, 455208.
- 683 Salmon, P. S., Barnes, A. C., Martin, R. A., and Cuello, G. J. (2006). Glass fragility and atomic  
684 ordering on the intermediate and extended range. *Phys. Rev. Lett.* 96, 235502.
- 685 Salmon, P. S., and Liu, J. (1994). The relation between the melt topology and glass-forming ability for  
686 liquid Ge-Se alloys. *J. Phys.: Condens. Matter* 6, 1449–1460.
- 687 Salmon, P. S., Martin, R. A., Mason, P. E., and Cuello, G. J. (2005). Topological versus chemical  
688 ordering in network glasses at intermediate and extended length scales. *Nature* 435, 75–78.
- 689 Salmon, P. S., and Petri, I. (2003). Structure of glassy and liquid GeSe<sub>2</sub>. *J. Phys.: Condens. Matter*  
690 15, S1509–S1528.
- 691 Salmon, P. S., and Zeidler, A. (2013). Identifying and characterising the different structural length scales  
692 in liquids and glasses: An experimental approach. *Phys. Chem. Chem. Phys.* 15, 15286–15308.
- 693 Sarrach, D. J., De Neufville, J. P., and Haworth, W. L. (1976). Studies of amorphous Ge-Se-Te alloys  
694 (I): Preparation and calorimetric observations. *J. Non-Cryst. Solids* 22, 245–267.
- 695 Sartbaeva, A., Wells, S. A., Huerta, A., and Thorpe, M. F. (2007). Local structural variability and the  
696 intermediate phase window in network glasses. *Phys. Rev. B* 74, 224204.
- 697 Savage, J. A., and Nielsen, S. (1965). Chalcogenide glasses transmitting in the infrared between 1 and  
698 20 μ – a state of the art review. *Infrared Phys.* 5, 195–204.
- 699 Schawe, J. E. K. (1995). A comparison of different evaluation methods in modulated temperature DSC.  
700 *Thermochimica Acta* 260, 1–16.
- 701 Sears, V. F. (1992). Neutron scattering lengths and cross sections. *Neutron News* 3, 26–37.
- 702 Senapati, U., and Varshneya, A. K. (1995). Configurational arrangements in chalcogenide glasses: A  
703 new perspective on Phillips’ constraint theory. *J. Non-Cryst. Solids* 185, 289–296.
- 704 Senapati, U., and Varshneya, A. K. (1996). Viscosity of chalcogenide glass-forming liquids: An anomaly  
705 in the ‘strong’ and ‘fragile’ classification. *J. Non-Cryst. Solids* 197, 210–218.

- 706 Sharma, D., Sampath, S., Lalla, N. P., Awasthi, A. M. (2005). Mesoscopic organization and structural  
707 phases in network-forming  $\text{Ge}_x\text{Se}_{1-x}$  glasses. *Physica B* 357, 290–298.
- 708 Shatnawi, M. T. M., Farrow, C. L., Chen, P., Boolchand, P., Sartbaeva, A., Thorpe, M. F., and Billinge,  
709 S. J. L. (2008). Search for a structural response to the intermediate phase in  $\text{Ge}_x\text{Se}_{1-x}$  glasses.  
710 *Phys. Rev. B* 77, 094134.
- 711 Soper, A. K. (1991). First results from SANDALS – the Small Angle Neutron Diffractometer for  
712 Amorphous and Liquid Samples at ISIS. In Proceedings of the Eleventh Meeting of the International  
713 Collaboration on Advanced Neutron Sources ICANS-XI, Volume II. Ed. M. Misawa, M. Furusaka,  
714 H. Ikeda, N. Watanabe. KEK Report 90-25, Tsukuba, Japan. pp 809–819.
- 715 Soper, A. K. (2011). GudrunN and GudrunX: Programs for correcting raw neutron and X-ray diffraction  
716 data to differential scattering cross section. Rutherford Appleton Laboratory Technical Report  
717 RAL-TR-2011-013.
- 718 Sreeram, A. N., Swiler, D. R., and Varshneya, A. K. (1991a). Gibbs-DiMarzio equation to describe the  
719 glass transition temperature trends in multicomponent chalcogenide glasses. *J. Non-Cryst. Solids*  
720 127, 287–297.
- 721 Sreeram, A. N., Varshneya, A. K., and Swiler, D. R. (1991b). Molar volume and elastic properties of  
722 multicomponent chalcogenide glasses. *J. Non-Cryst. Solids* 128, 294–309.
- 723 Stølen, S., Grande, T., and Johnsen, H.-B. (2002). Fragility transition in  $\text{GeSe}_2$ -Se liquids. *Phys. Chem.*  
724 *Chem. Phys.* 4, 3396–3399.
- 725 Stølen, S., Johnsen, H. B., Bøe, C. S., Grande, T., and Karlsen, O. B. (1999). Stable and metastable  
726 phase equilibria in the  $\text{GeSe}_2$ -Se system. *J. Phase Equilibria* 20, 17–28.
- 727 Svoboda, R., and Málek, J. (2015). Kinetic fragility of Se-based binary chalcogenide glasses. *J. Non-*  
728 *Cryst. Solids* 419, 39–44.
- 729 Thorpe, M. F. (1983). Continuous deformations in random networks. *J. Non-Cryst. Solids* 57, 355–370.
- 730 Thorpe, M. F., Jacobs, D. J., Chubynsky, M. V., and Phillips, J. C. (2000). Self-organization in network  
731 glasses. *J. Non-Cryst. Solids* 266-269, 859–866.
- 732 Wagner, T., Kasap, S. O., and Maeda, K. (1997). Glass transformation, heat capacity, and  
733 structure of  $\text{Ge}_x\text{Se}_{100-x}$  glasses studied by temperature-modulated differential scanning calorimetry  
734 experiments. *J. Mater. Res.* 12, 1892–1899.
- 735 Wang, F., Boolchand, P., and Micoulaut, M. (2000). Glass structure, rigidity transitions and the  
736 intermediate phase in the Ge-As-Se ternary. *Europhys. Lett.* 52, 633–639.
- 737 Wang, F., Mamedov, S., Boolchand, P., Goodman, B., and Chandrasekhar, M. (2005). Pressure Raman  
738 effects and internal stress in network glasses. *Phys. Rev. B* 71, 174201.
- 739 Wang, Y., Ohata, E., Hosokawa, S., Sakurai, M., Matsubara, E. (2004). Intermediate-range order in  
740 glassy  $\text{Ge}_x\text{Se}_{1-x}$  around the stiffness transition composition. *J. Non-Cryst. Solids* 337, 54–61.
- 741 Yang, Y., Gulbiten, O., Gueguen, Y., Bureau, B., Sangleboeuf, J.-C., Roiland, C., King, E. A., and  
742 Lucas, P. (2012). Fragile-strong behavior in the  $\text{As}_x\text{Se}_{1-x}$  glass forming system in relation to  
743 structural dimensionality. *Phys. Rev. B* 85, 144107.
- 744 Yang, G., Gueguen, Y., Sangleboeuf, J.-C., Rouxel, T., Boussard-Plédel, C., Troles, J., Lucas, P.,  
745 and Bureau, B. (2013). Physical properties of the  $\text{Ge}_x\text{Se}_{1-x}$  glasses in the  $0 < x < 0.42$  range in  
746 correlation with their structure. *J. Non-Cryst. Solids* 377, 54–59.
- 747 Yildirim, C., Raty, J.-Y., and Micoulaut, M. (2016a). Revealing the role of molecular rigidity on the  
748 fragility evolution of glass-forming liquids. *Nature Comm.* 7, 11086.
- 749 Yildirim, C., Raty, J.-Y., and Micoulaut, M. (2016b). Anomalous diffusion and non-monotonic  
750 relaxation processes in Ge-Se liquids. *J. Chem. Phys.* 144, 224503.
- 751 Zeidler, A., and Salmon, P. S. (2016). Pressure-driven transformation of the ordering in amorphous  
752 network-forming materials. *Phys. Rev. B* 93, 214204.
- 753 Zhao, H. Y., Koh, Y. P., Pyda, M., Sen, S., and Simon, S. L. (2013). The kinetics of the glass transition  
754 and physical aging in germanium selenide glasses. *J. Non-Cryst. Solids* 368, 63–70.
- 755 Zheng, Q., Mauro, J. C., Ellison, A. J., Potuzak, M., and Yue, Y. (2011). Universality of the high-  
756 temperature viscosity limit of silicate liquids. *Phys. Rev. B* 83, 212202.

- 757 Zheng, Q., Mauro, J. C., and Yue, Y. (2017). Reconciling calorimetric and kinetic fragilities of glass-  
758 forming liquids. *J. Non-Cryst. Solids* 456, 95–100.
- 759 Zhou, W., Paesler, M., and Sayers, D. E. (1991). Structure of germanium-selenium glasses: An x-ray-  
760 absorption fine-structure study. *Phys. Rev. B* 43, 2315–2321.